AN ADAPTIVE GM-C FILTER BASED POST-EQUALIZER FOR WIDE-BAND VISIBLE LIGHT COMMUNICATION SYSTEMS

by

Emrah Haydar

B.S., Electrical Engineering, Yıldız Technical University, 2017

B.S., Electronics & Communications Engineering, Yıldız Technical University, 2018

Submitted to the Institute for Graduate Studies in
Science and Engineering in partial fulfillment of
the requirements for the degree of
Master of Science

Graduate Program in Electrical & Electronics Engineering
Boğaziçi University
2022

ACKNOWLEDGEMENTS

I would like to express my deepest gratitude to my supervisor, Arda Deniz Yalçınkaya for his guidance and wisdom throughout my studies and thesis project. I would also like to thank my friends and family for their encouragement and support during my M.S. study.

ABSTRACT

AN ADAPTIVE GM-C FILTER BASED POST-EQUALIZER FOR WIDE-BAND VISIBLE LIGHT COMMUNICATION SYSTEMS

Visible Light Communication (VLC), more commonly known as Li-Fi (Light Fidelity), has been a buzzword since it was first introduced by Harald Haas in 2011. The idea is that a light source can be used as both illumination and communication means. By switching the current of an LED at high speed, data transmission can be performed and the human eye is not disturbed by the flickering. With the recent research in this field, benefits, challenges, and proven solutions have been addressed. One of the big challenges is the limited modulation bandwidth of the transmitter LED which predominantly determines the achievable maximum data rate. Literature review shows that for the white LEDs, the modulation bandwidth is in the range of hundreds of kHz and a few MHz. Methods to extend the modulation bandwidth includes using: coding/modulation schemes, pre-equalizer, lenses/filters, and post equalizers. Among them, a post equalizer is most easily implemented as it deals with small signals at the receiver side. It can be realized with basic or active RC networks and as well as with ANNs as recent works show.

In this work, a Gm-C filter-based post equalizer topology has been proposed. By employing 3-bit capacitors, the equalizer can provide eight distinct edge frequencies which correspond to modulation bandwidths of LEDs in the range of 0.7MHz to 5MHz and at least tenfold equalization is achieved. The circuit is realized by using 130nm low threshold MOSFETs and consumes only $240\mu W$. The overall chip area is $340\times340\mu m^2$. Post layout simulations, with eye diagrams, show that data rate up to 200MBits is achievable given that a 5MHz modulation bandwidth is available at the receiver side.

ÖZET

GENİŞ BANT GÖRÜNÜR IŞIK HABERLEŞME SİSTEMLERİ İÇİN UYARLANABİLİR GM-C FİLTRE TABANLI BİR ART-DENKLEŞTİRİCİ

2011'deki Harald Haas tarafından ilk tanıtımından sonra, Görünür Işık Haberleşmesi ya da daha yaygın bir isimle Li-Fi, bilindik bir kelime olmuştur. Bir ışık kaynağının hem aydınlatma hem de haberleşme aracı olarak kullanılabilmesi prensibine dayalı bir fikirdir. LED akımının yüksek hızlarda anahtarlanması sayesinde veri aktarımı mümkün olabilirken insan gözü ise ışığın titremesinden rahatsız olmaz. Son yıllarda yapılan araştırmalarla, avantajları, zorlukları ve kanıtlanmış çözümleri ele alınmıştır. En büyük sorunlardan birisi kullanılan LED'in sınırlı modülasyon bant genişliğidir. Öyle ki kullanılan LED, büyük ölçüde, azami veri hızını belirlemektedir. Literatür taraması gösteriyor ki, beyaz LED'ler için modülasyon bant genişliği birkaç yüz kHz ila birkaç MHz arasındadır. Kodlama/modülasyon teknikleri, ön-denkleştirici, lens/filtre ve art-denkleştirici kullanmak bant genişliğini artıran yöntemlerdir. Bunların içinde art-denkleştirici yapıları küçük sinyallerle işlem yaptığından, basit veya aktif RC devrelerle ve hatta YSA ile bile gerçekleştirilmesi mümkündür.

Bu tez çalışmasında, Gm-C filtre tabanlı bir art-denkleştirici sunulmuştur. 3-bit'lik kapasiteler sayesinde 0.7-5MHz arasında değişen LED modülasyon bant genişliğine denk gelen sekiz farklı köşe frekansı ve en az on kat denkleştirme sağlamaktadır. Devre, 130nm düşük eşik gerilimli MOSFET'ler kullanılarak gerçekleştirilmiştir ve sadece $240\mu W$ güç harcamaktadır. Toplam serim alanı $340\times340\mu m^2$'dir. Serim sonrası göz diyagramı simülasyonlarında, eğer alıcı tarafta 5MHz modülasyon bant genişliği mevcutsa, 200MBit'e kadar veri aktarımının mümkün olabileceği gösterilmiştir.

TABLE OF CONTENTS

LIST OF FIGURES

LIST OF TABLES

LIST OF SYMBOLS

A	Voltage Gain
f	Frequency in Hertz
g_m	Transconductance
$H_X(s)$	Transfer Function of a Given System X
j	Imaginary Unit
k_{eq}	Equalization Factor
R_p	Pass Band Ripple
z	Small Signal Impedance
Z	Impedance
s	Laplace Domain Variable
α	Real Part of a Complex Root
β	Imaginary Part of a Complex Root
ρ	Complex Root of an s-Domain Equation
ω	Radial Frequency
Ω	Ohm: Unit of Resistance
$\implies$	Implies (If True, Then)
$\rightarrow$	Approaches to (In Limit)
$:=$	Definition
$\propto$	Proportional to, Related to

LIST OF ACRONYMS/ABBREVIATIONS

ANN	Artificial Neural Network
CMFB	Common-Mode-Feed-Back
DNN	Deep Neural Network
EM	Electro-Magnetic
LD	Laser Diode
LED	Light Emitting Diode
Li-Fi	Light Fidelity
LPF	Low Pass Filter
MBits	Mega Bits per Second
MIM	Metal-Insulator-Metal (a Capacitor)
MOM	Metal-Oxide-Metal (a Capacitor)
NUM	Numerator
OOK	On-Off Keying
OTA	Operational Transconductance Amplifier
PEQ	Post EQualizer
RMS	Root Mean Square
RSS	Received Signal Spectrum
STC	Single Time Constant
TA	Transconductance Amplifier
TIA	Trans-Impedance Amplifier
VLC	Visible Light Communication
YSA	Yapay Sinir Ağı

1. INTRODUCTION

Visible Light Communication (VLC) has been a hot research field in recent years due to its promising applications. Although VLC is a general term for transmitting data with the visible part of the EM spectrum, the main interest in this field is using indoor LEDs for both communication and illumination purposes [1,2]. Because the cost of commercially available LEDs decreases while the efficiency and other performance parameters improve [3].

Many studies in this field assess its potential profits, main challenges, and proven solutions. One of the big challenges is the limited modulation bandwidth of the transceiver LED. Studies show that the measured bandwidth of the signal at the receiver side depends dominantly on the type of LED employed. This is reported as 3-5MHz for phosphorus-based LEDs [4], about 10MHz for single-color LEDs [5] and another study shows that for single color LEDs, it is 5.3MHz, 5.7MHz and 6.6MHz for green, red and blue components respectively [6]. For μLEDS, it can be as high as dozens of MHz and at extremes, LDs have the largest bandwidth beyond 1GHz [5]. For white LEDs, 2.2MHz and below 3MHz bandwidths are reported [5] and also it can be as low as 0.7MHz [7]. For the use of LEDs for both illumination and communication, our interest can be narrowed down to white LEDs which can be realized by either using separate RGB LEDs or blue emitters combined with phosphorus [4].

The above discussion yields the main result that the LEDs, which are used for both illumination and communication, have modulation bandwidth within the range of hundreds of kHz to a few MHz. Which, in return, defines the data rate which can be achieved. In their studies, researchers also provided the solutions to broaden the bandwidth thus the data rate of the VLC transceiver system. Consider the basic VLC transceiver system given in Figure 1.1 to describe the possible solutions.

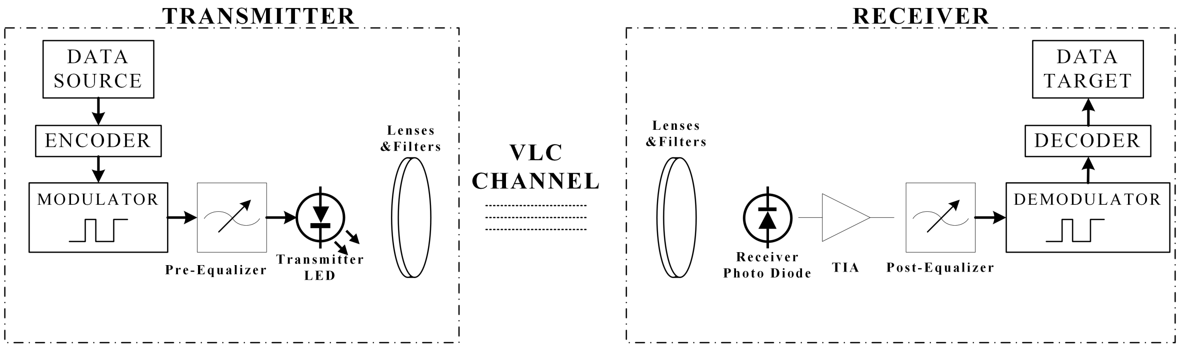

Figure 1.1. Generic VLC transceiver system.

The operation of the transceiver system can be put into words as follows:

(i) At the transmitter side:
- Data from the source is encoded and modulated in accordance with the preferred scheme.
- A pre-equalizer is used to boost the high-frequency components of the signal to compensate for the limited bandwidth of the transmitter LED.
- LED turns the pre-equalized electrical signal into an optical signal.
- Optical lenses and/or filters employed to condition the light for illumination and to filter some of the light components.

(ii) Light signal transmitted along VLC channel which can be vacuum/air or water depending on the application.

(iii) At the receiver side:
- Lenses/filters can be used for filtering and focusing the incoming light.
- Receiver photo-diode turns the optical signal into an electrical current signal.
- Trans Impedance Amplifier (TIA) converts the current signal into a voltage signal.
- Post-equalizer is used to broaden the received signal spectrum to a target frequency (equalize the bandwidth).
- Signal is then demodulated and decoded before feeding into the target (signal processor).

The improvement can be made in various stages in the transceiver system to broaden the bandwidth and thus data rate. These improvements can be applied in combinations to provide further enhancement. Proved solutions are described in the following section.

1.1. Methods to Enhance the Modulation Bandwidth

1.1.1. Coding and Modulation Schemes

These methods make it possible to achieve data rates which is greater than simple On/Off Keying with available bandwidth rather than physically enhancing the bandwidth.

1.1.2. Pre-Equalization

Pre-equalizer or pre-emphasis circuits are used to supply a large and high-speed signal current for Illumination and high-speed data transmission. It can be realized with resonant circuits [8], T-Bridge circuits [1, 9] and weighted pre-equalization [2]. Such circuit uses RLC or RC components combined with active devices such as Op-Amps or discrete transistors to achieve higher transmitted powers.

1.1.3. Using Lenses-Filters

Optical filters/lenses are utilized at both sides of the transceiver system for reasons: conditioning light for illumination [5], focusing [1, 2, 4, 7, 10–12] and filtering out low frequency components [1, 10], which simply filters out the slow yellow component (blue filter) [2, 3, 11, 13]. It is important to note that the utilization of filters has the disadvantage of additional costs and non-feasibility for widespread use [5, 6].

1.1.4. Post Equalization

Although the combination of the aforementioned methods is used to enhance the bandwidth, researchers also preferred to use a Post Equalizer (PEQ) to provide additional bandwidth on the received signal spectrum. PEQs are similar to pre-equalizers but require less-complex circuits and less power to operate as it deals with small signals at the receiver side. In literature, many methods have been proven to realize a PEQ.

A simple first-order RC network can be used to equalize the bandwidth of the received signal [3,6]. In the VLC transceiver system shown in Figure1.2, the received light signal is focused and the yellow component is blocked leaving only the blue component. The blue component has a bandwidth of 14MHz and it is equalized to 50MHz by using a post equalizer which is realized with a capacitor in parallel with a resistor (signal is pre-amplified in TIA stage). 100MBits data rate is achieved using OOK-NRZ scheme. It is important to note that the overall equalizer response depends also on the load impedance.

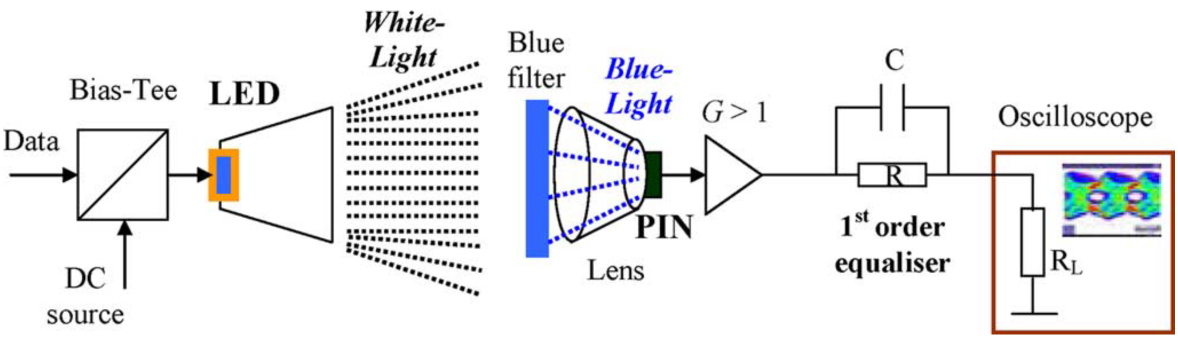

Figure 1.2. A simple (passive) RC PEQ [3].

Active components can be used along with simple RC networks to add more gain on the received signal or at least to avoid signal attenuation [5, 11, 12]. In the PEQ circuits given in Figure1.3(a) and Figure1.3(b), the same author later used a two-stage CTLE (Continuous Time Linear Equalizer) with a similar circuit. The circuit in the Figure1.3(b) provides variable edge frequencies by employing variable capacitors (2-bit capacitors) and about tenfold equalization (from 2.2MHz to 20MHz). The circuit also provides a signal gain of about 36dB at TIA stage.

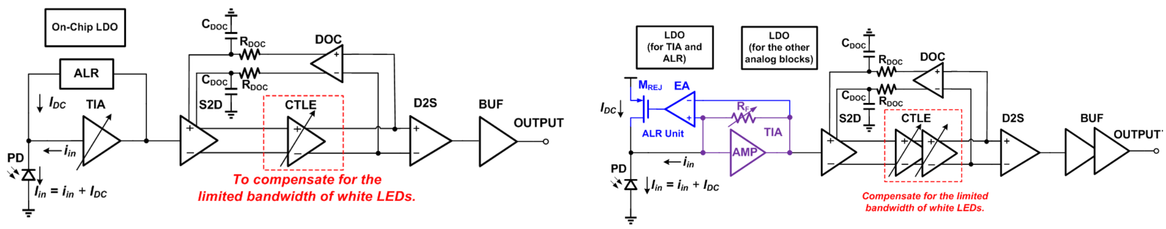

(a) (b)

Figure 1.3. Active RC PEQs realized with Op-Amps [5].

In another paper [12], the author realized the PEQ with common-emitter and emitter follower amplifiers realized with discrete transistors. The adjustment of the edge frequency of the PEQ is carried out by varying the components R_1, R_2, C_3 and C_4. After some optimization, the author achieved the best equalization from 94MHz to 815MHz.

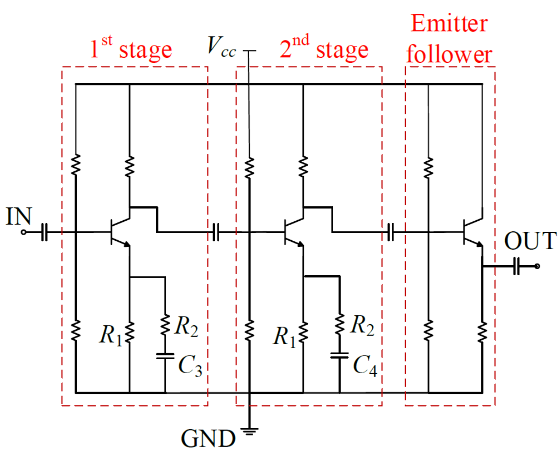

Figure 1.4. Active RC PEQ realized with discrete transistors [12].

Also, passive RC and active RC PEQs can be used in combination [4, 11]. The circuit given in the Figure1.5(a) is realized with two passive RC and one active RC networks. Filtered light signal has a bandwidth of 12MHz (blue component) and it is equalized to about 150MHz. 340MBits data rate is achieved using OOK-NRZ scheme. In the other work [11], the author employed cascaded passive and active RC networks to implement the PEQ. With a white LED, the data rate is extended from 28MBits to 75MBits (the bandwidth of the blue component is reported as 12MHz).

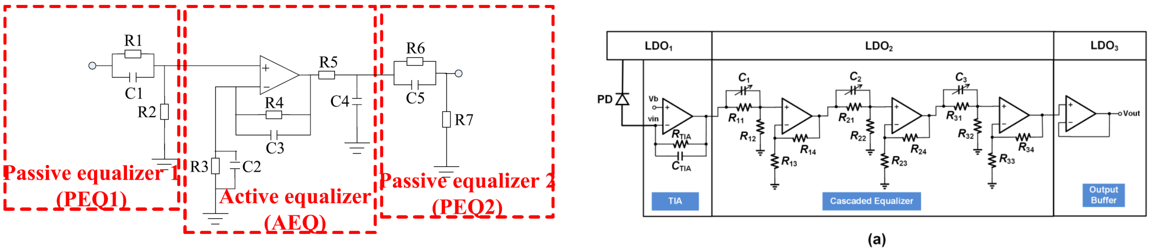

(a) (b)

Figure 1.5. Combined passive and active RC PEQs [4, 11].

1.1.5. Artificial Neural Network Based Equalization

ANN/DNN (Artificial/Deep Neural Network) based equalization [1, 10, 14–16] requires training data that should be available for a given transceiver system. There are drawbacks to using ANN for equalization, such as training times and convergence might be problematic depending on the transmitter topology [15, 16].

Among the methods given above, passive or active RC PEQs are most suitable due to their easy analysis and implementation. It is clear that these filters are linear, meaning, the designers assumed that the Received Signal Spectrum (RSS) has a linear Low Pass Filter (LPF) behavior after the cut-off frequency.

Authors in papers [5, 7], assumed 1st order LPF behavior model for the RSS and designed the PEQs accordingly. In another paper [3], the author fitted the LED response with an exponential function, but utilized a 1st order equalizer to approximate this behavior. Although the received signal spectrum has more complex behavior than a simple 1st order linear model, these studies show that this assumption still yields improvement on the date rates achieved. Figure 1.6 shows the described assumption and required PEQ response.

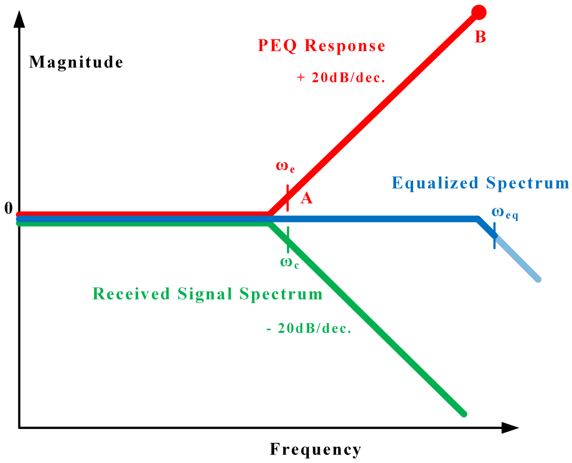

Figure 1.6. The assumption for RSS, required PEQ response and equalized spectrum.

In Figure1.6, ω_c and ω_e are the cut-off frequency of the RSS and edge frequency of the PEQ respectively. PEQ circuit works against -20dB/decade roll-off rate of the signal amplitude after the cut-off frequency. Therefore, it is straightforward to see also from Figure 1.6 that the slope of the PEQ curve should be +20dB/decade and $\omega_e = \omega_c$. In a mathematical form, received signal spectrum: $H_{RSS}(s)$ and required PEQ response: $H_{EQ}(s)$ can be described as

$$H_{RSS}(s) = \frac{A_0}{1 + \frac{s}{\omega_c}},$$
$$H_{EQ}(s) = \left(1 + \frac{s}{\omega_e}\right) \times \frac{1}{H^*}.$$

Here, A_0 and ω_c describe the low frequency (DC) magnitude and cut-off frequency of the RSS, $\omega_e = \omega_c$ is the edge frequency of the equalizer and H^* models the non-ideal behavior of the PEQ. Ideally, if $H^* = 1$, the equalized bandwidth would be infinite. In a practical case, H^* determines the overall equalizer response. For example, it might describe the behavior of the PEQ after point B in Figure 1.6, due to the limited bandwidth of the equalizer itself. In return, it determines the maximum equalized bandwidth achievable. To put it mathematically, the output of the PEQ (equalized spectrum) becomes

$$\begin{aligned}
H_{OUT}(s) &= H_{RSS}(s) \times H_{EQ}(s), \\
&= \frac{A_0}{1+\frac{s}{\omega_c}} \times \left(1+\frac{s}{\omega_e}\right) \times \frac{1}{H^*}, \\
&= \frac{A_0}{H^*}.
\end{aligned}$$

The details of the equalization process will be described in Section 2.1.

1.2. Contribution of This Thesis Study

In this work, we propose a Gm-C filter-based 1st order PEQ circuit that can provide equalization for various cases. We considered the received signal spectrums with cut-off frequencies in the range of 700kHz to 5MHz and aimed for a maximum equalized bandwidth around 100MHz. To meet various cut-off frequencies of the received signals, a 3-bit capacitor is used to provide $2^3 = 8$ distinct edge frequencies. This method adds flexibility to the PEQ filter design and provides a digital control mechanism.

There are Gm-C filter-based equalizer topologies in literature (mainly, application specific). 2nd order equalizers (with two zeros) are implemented, as a general channel equalizer [17], as a cable equalizer for a 100Base-TX application [18] and as a bump equalizer for low voltage applications [19]. In another work, a programmable 1st order equalizer is implemented for a 1000BASE-T application as a cable equalizer [20]. In the next section, we described how the proposed circuit is obtained to have the required PEQ response, provided analysis for the practical case, and finally specify the parameters for the practical design.

2. PROPOSED POST EQUALIZER CIRCUIT

In this chapter, we describe the roadmap of how the proposed PEQ is obtained and analyzed for practical application. Firstly, it is important to remark that we abide by the assumptions described in Figure1.6. Then, we try and obtain the required PEQ response with a Gm-C topology. For the practical application, we preferred to employ a simple but effective model for the Gm-Cell in the Section2.1. Finally, we performed hand analysis for the practical case and determine the necessary parameters (gain and bandwidth) expected from the Gm-Cell. For a given specific equalization process, we also provided quantitative values for the Gm-Cell.

Before introducing the proposed circuit, consider two useful circuits given in Figure 2.1(a) and Figure 2.1(b). These circuits are realized using ideal fully differential Transconductance Amplifier (TA or OTA: Operational Transconductance Amplifier, or more conventionally called a Gm-Cell) as shown in Figure 2.1(c) which has the terminal relationship given as: $I_o = g_m(v_{in+} - v_{in-})$. Here, g_m is the transconductance and I_o is the differential output current, it sources from one terminal and sinks into the other.

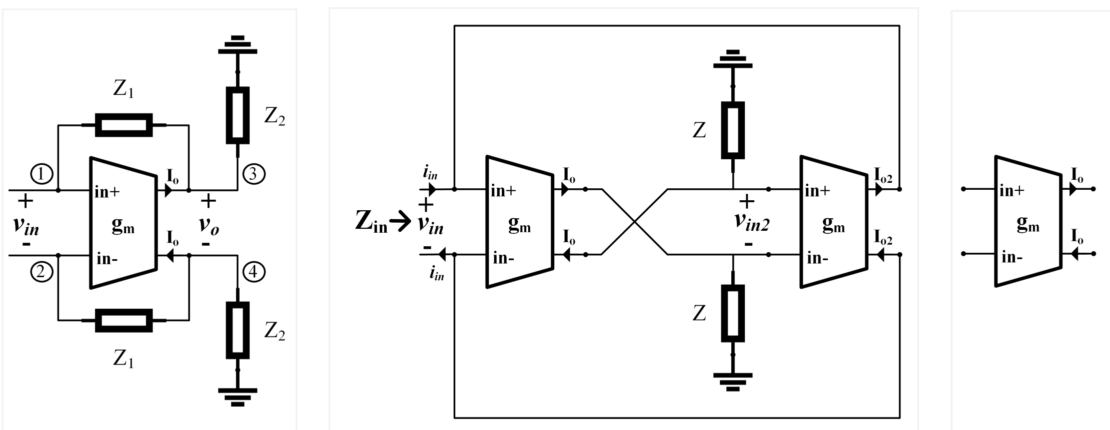

(a) (b) (c)

Figure 2.1. A basic Gm-Z circuit (a), impedance converter (b) and ideal OTA (c).

Let us perform a node analysis for the circuit in Figure 2.1(a). We can write

$$\frac{v_1 - v_3}{Z_1} + I_o = \frac{v_3}{Z_2}, \tag{2.1}$$

and

$$\frac{v_2 - v_4}{Z_1} - I_o = \frac{v_4}{Z_2}. \tag{2.2}$$

For the OTA, we can write

$$\begin{aligned} I_o &= g_m(v_{in+} - v_{in-}), \\ &= g_m(v_1 - v_2). \end{aligned} \tag{2.3}$$

By the subtraction of Equation(2.1) - Equation(2.2) and substituting Equation(2.3), we obtain

$$\begin{aligned} \frac{v_1 - v_2}{Z_1} - \frac{v_3 - v_4}{Z_1} + 2I_o &= \frac{v_3 - v_4}{Z_2}, \\ V_{in} &= v_1 - v_2, \\ V_o &= v_3 - v_4, \\ V_{in}\left(\frac{1}{Z_1} + 2g_m\right) &= V_o\left(\frac{1}{Z_1} + \frac{1}{Z_2}\right). \end{aligned}$$

The transfer function becomes

$$\begin{aligned} H(s) :&= \frac{V_o}{V_{in}}, \\ &= \frac{\frac{1}{Z_1} + 2g_m}{\frac{1}{Z_1} + \frac{1}{Z_2}}. \end{aligned} \tag{2.4}$$

If we choose $Z_2 = \infty$ (open circuit) and $Z_1 = sL$ (inductor), $H(s) = 1 + 2g_m sL$. This is the desired 1st order equalizer response with an edge frequency of $\omega_e = \frac{1}{2g_m L}$. In a Gm-C filter topology, it is illegal to use any passive component other than capacitors (including inductors). But, we may use a floating pseudo-inductor (also named gyrator). For that purpose, consider the impedance converter circuit in Figure 2.1(b), $I_o = g_m V_{in}$. For the second OTA

$$\begin{aligned}
V_{in2} &= -2 \times Z I_o, \\
&= -2 Z g_m V_{in}, \\
I_{o2} &= g_m V_{in2}, \\
&= -2 g_m^2 Z V_{in}.
\end{aligned}$$

Input differential impedance becomes

$$Z_{in} := \frac{V_{in}}{I_{in}} = -\frac{V_{in}}{I_{o2}} = \frac{1}{2 g_m^2 Z}. \tag{2.5}$$

This simply implies that this circuit provides the reciprocal of an impedance. In case $Z = \frac{1}{sC}$ (then it becomes a pseudo-inductor/gyrator), $Z_{in} = \frac{sC}{2g_m^2}$. This is the impedance of an inductor with the equivalent inductance of

$$L_{eq} = \frac{C}{2 g_m^2}.$$

Now we can combine these two circuits to obtain the proposed PEQ topology as shown in Figure 2.2, which has the transfer function of

$$\begin{aligned}
H(s) &= 1 + 2 G_m s L_{eq}, \\
&= 1 + 2 G_m s \frac{C}{2 g_m^2}.
\end{aligned}$$

Here, we employ identical transconductance for both gyrators and main amplifier, $G_m = g_m$, which yields a simple transfer function of

$$H(s) = 1 + \frac{sC}{g_m}. \tag{2.6}$$

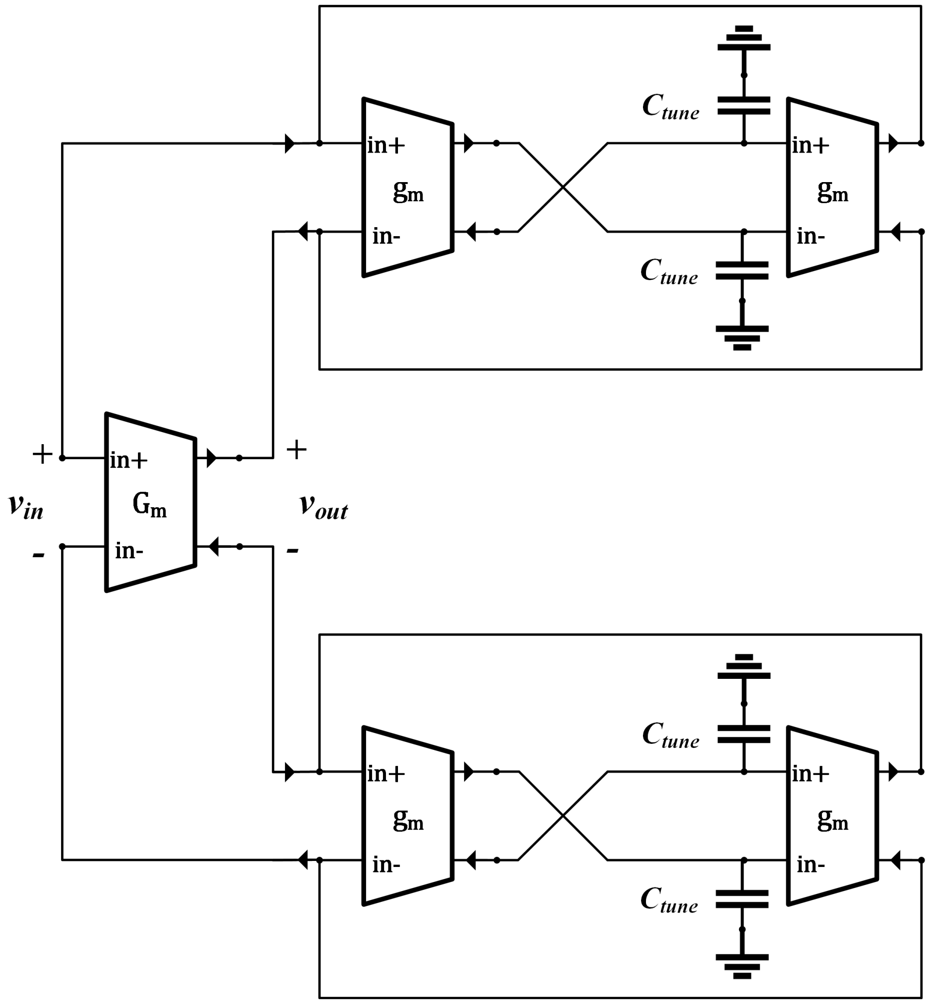

Figure 2.2. Proposed Gm-C PEQ circuit.

Thus, the edge frequency of the PEQ becomes $\omega_e = \frac{g_m}{C}$. The tuning of the edge frequency can be carried out by two means, namely, g_m or C. Tuning with g_m is performed in a continuous manner. For a given OTA circuit topology and bias current, the adjustment range of g_m is restricted and change in g_m will also affect the bandwidth of OTA. Tuning with an n-bit capacitor array provides a free tuning range with a resolution defined by

$$C_{step} = \frac{C_{max} - C_{min}}{2^n}.$$

2.1. Practical Case

In practice, with whatever method a Gm-Cell is realized, it has limited bandwidth and limited open-load voltage gain.

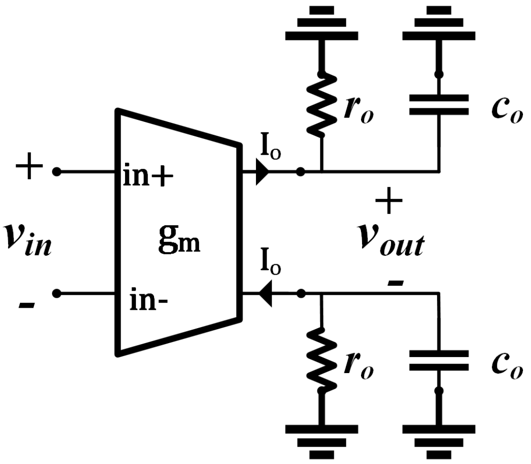

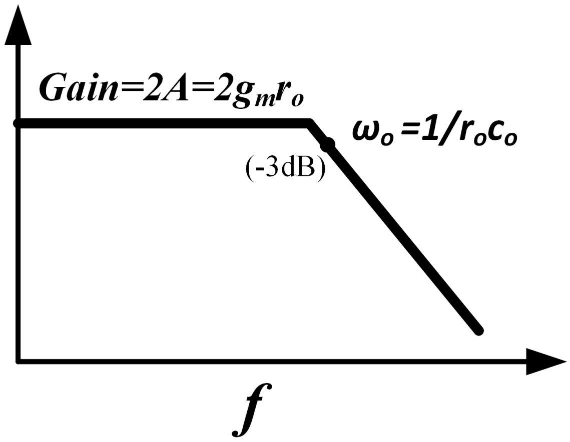

(a) (b)

Figure 2.3. Practical Gm-Cell circuit (a) and its Bode-Plot (b).

Both limitations can be modeled with the equivalent circuit given in Figure 2.3(a). To find the gain function of this circuit, one should consider the following

$$\begin{aligned} z_o &= r_o \parallel \frac{1}{sc_o} = \frac{r_o}{1+sr_oc_o}, \\ V_o &= 2 \times z_oI_o = 2 \times \frac{r_o}{1+sr_oc_o} g_mV_{in}, \\ \frac{V_o}{V_{in}} &= \frac{2g_mr_o}{1+sr_oc_o}. \end{aligned}$$

Defining open load DC voltage gain (single end) and bandwidth of Gm-Cell as $A := g_mr_o$ and $\omega_o := \frac{1}{r_oc_o}$ respectively,

$$\frac{V_o}{V_{in}} = \frac{2A}{1+\frac{s}{\omega_o}},$$

which has the magnitude Bode plot as shown in Figure 2.3(b). Although this model seems too simple, later in this paper, it will be shown that for given Gm-Cell topology this assumption holds true up to the frequencies of interest. Now, let us realize the gyrator with practical Gm-Cells as shown in Figure 2.4. A simplified Laplace version of the circuit is given in Figure 2.5.

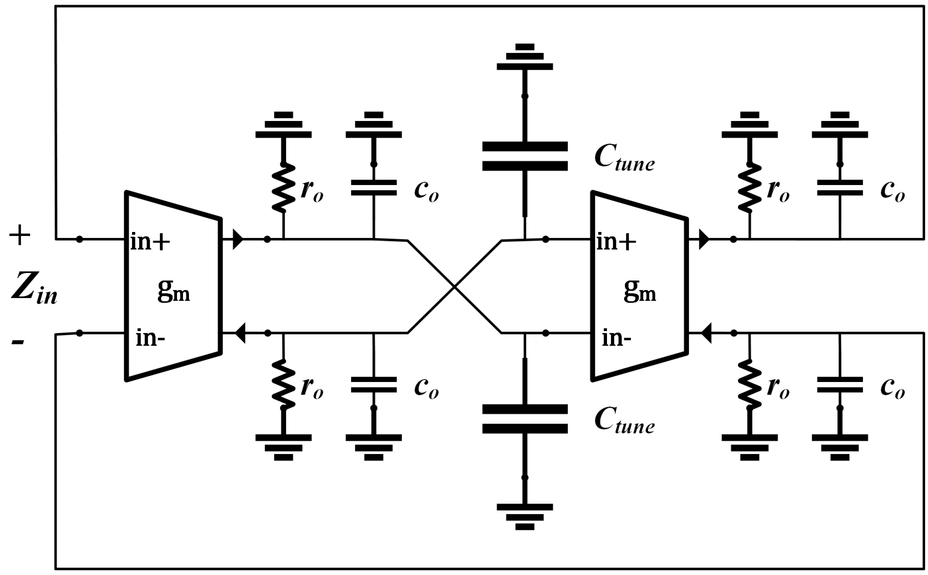

Figure 2.4. Gyrator realized with practical Gm-Cells.

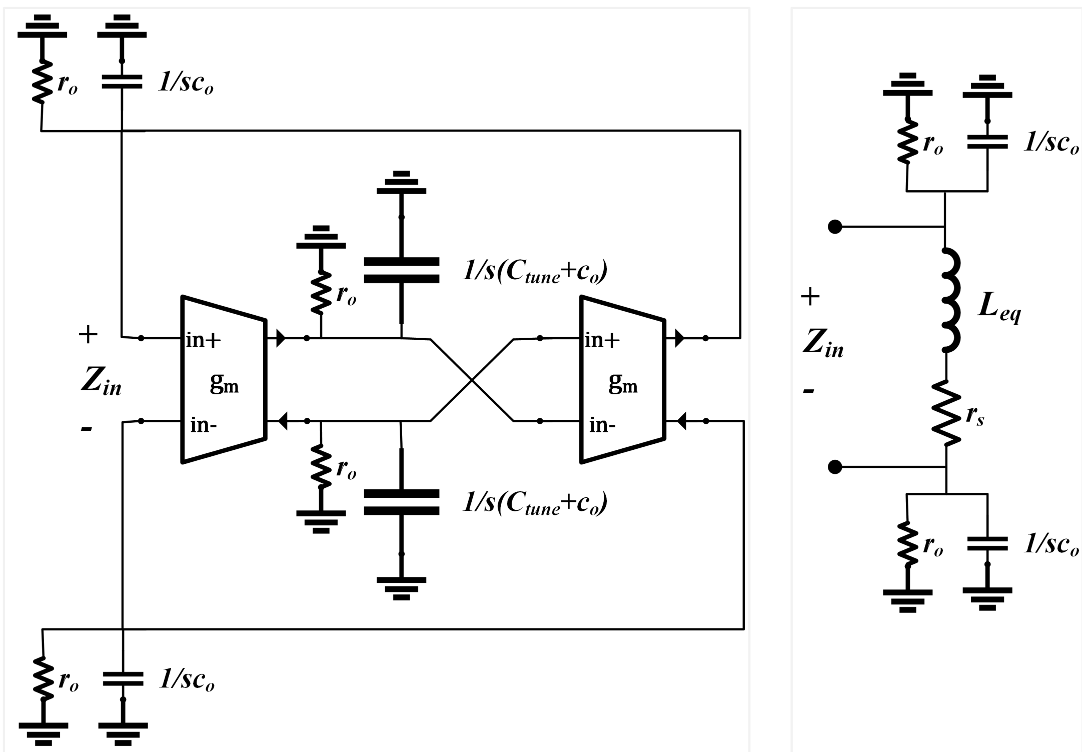

(a) (b)

Figure 2.5. Laplace domain (a) and equivalent (b) version of practical gyrator.

Using the impedance converter formula (Equation(2.5)), we obtain

$$
\begin{aligned}
Z_{in,diff} &= \frac{1}{2g_m^2 Z} = \frac{1}{2g_m^2\left(r_o \parallel \frac{1}{s(C_{tune}+c_o)}\right)}, \\
C_{tune} + c_o &\approx C_{tune}, \quad (C_{tune} \gg c_o), \\
Z_{in,diff} &= \frac{1}{2g_m^2}\left(\frac{1}{r_o} + sC_{tune}\right), \\
&= \frac{r_o}{2g_m^2 r_o^2} + \frac{sC_{tune}}{2g_m^2}, \\
&= \frac{r_o}{2A^2} + \frac{sC_{tune}}{2g_m^2},
\end{aligned}
$$

which resembles a real inductor with an equivalent inductance and a series resistance given respectively as

$$
\begin{aligned}
L_{eq} &= \frac{C_{tune}}{2g_m^2}, \\
r_s &= \frac{r_o}{2A^2},
\end{aligned}
$$

and with node to ground parasitic resistance and capacitance given as $r_p = r_o$ and $c_p = c_o$. Now let us apply this result to the Gm-C PEQ circuit as shown in Figure 2.6. Consider that the signal source has a low impedance, $r_{sig} \approx 0$ (i.e. the signal source is well-buffered), so we can ignore the pole resulting from $r_{sig} - z_o$ network at the input node. Observe that z_o of gyrator and main amplifier appears in parallel which reduces to $\frac{z_o}{2}$. And lastly, assume that there is no additive load, especially capacitive, at the output node (which means output is also buffered).

We chose identical Gm-Cells (thus, identical g_m, r_o and c_o) for both gyrators and main amplifier to obtain a simpler characteristic equation (transfer function) of the equalizer. If different Gm-Cells are used, the characteristic equation becomes too complex for hand analysis and one loses the insight into the equalizer behavior with respect to those parameters. Details will be given in the trade-offs section.

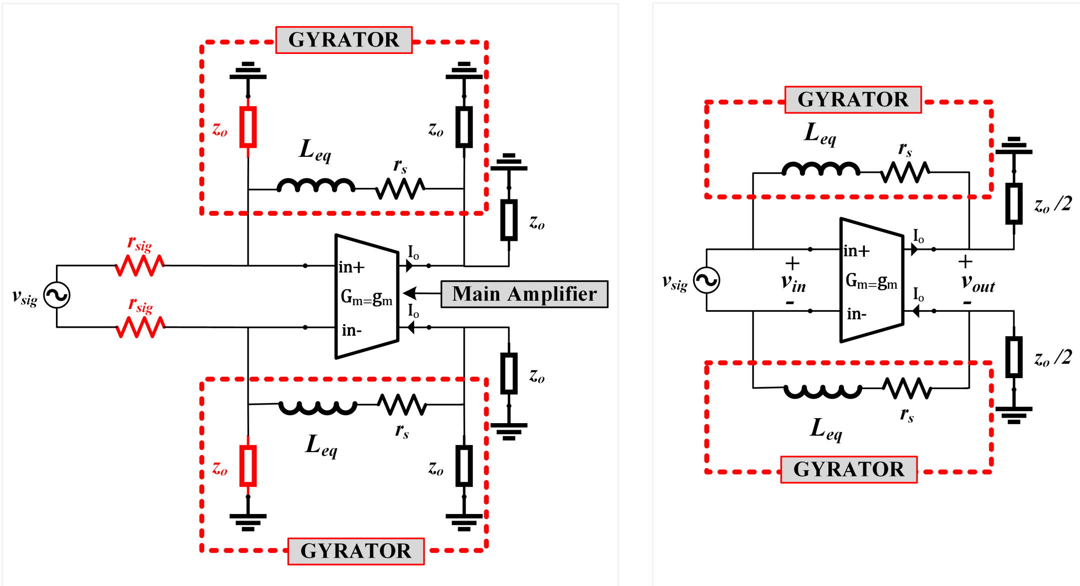

(a) (b)

Figure 2.6. Practical PEQ circuit (a) and simplified version (b).

We can apply the general Gm-Z formula (Equation(2.4)) to obtain the transfer function of the equalizer by substituting

$$
\begin{aligned}
Z_1 &= \frac{r_o}{2A^2} + \frac{sC_{tune}}{2g_m^2}, \\
Z_2 &= \frac{z_o}{2} = \frac{1}{2}\frac{1}{\frac{1}{r_o} + sc_o}, \\
H(s) &= \frac{\frac{1}{Z_1} + 2g_m}{\frac{1}{Z_1} + \frac{1}{Z_2}} = \frac{1 + 2g_m Z_1}{1 + \frac{Z_1}{Z_2}}, \\
&= \frac{1 + 2g_m\left(\frac{r_o}{2A^2} + \frac{sC_{tune}}{2g_m^2}\right)}{1 + \left(\frac{r_o}{2A^2} + \frac{sC_{tune}}{2g_m^2}\right) \times 2 \times \left(\frac{1}{r_o} + sc_o\right)}, \\
&= \frac{1 + \frac{2g_m r_o}{2A^2} + s\left(\frac{C_{tune}}{g_m}\right)}{1 + \frac{1}{A^2} + s\left(\frac{C_{tune}}{g_m^2 r_o} + \frac{c_o r_o}{A^2}\right) + s^2\left(\frac{C_{tune}c_o}{g_m^2}\right)}.
\end{aligned}
$$

By substituting $\omega_e = \frac{g_m}{C_{tune}}$, $\omega_o = \frac{1}{r_o c_o}$ and $A = g_m r_o$, we obtain

$$
H(s) = \frac{1 + \frac{1}{A} + s\frac{1}{\omega_e}}{1 + \frac{1}{A^2} + s\left(\frac{1}{A\omega_e} + \frac{1}{A^2\omega_o}\right) + s^2\frac{1}{A\omega_e\omega_o}}. \tag{2.7}
$$

For the ideal OTA case, $r_o \to \infty \implies A \to \infty$, $H(s) = 1 + \frac{s}{\omega_e}$. For non-ideal cases, we should examine the numerator and denominator parts separately for simplicity. Starting with the numerator part, finite gain (A) only affects the DC gain and has no effect on the edge frequency. Moreover, for relatively large A, we may approximate as

$$\begin{aligned} NUM(s) &= 1 + \frac{1}{A} + \frac{s}{\omega_e}, \\ &\approx 1 + \frac{s}{\omega_e}. \end{aligned}$$

For example, for $A = 10$, DC gain becomes $1 + \frac{1}{10} = 0.83dB$ (ideally should be zero). The denominator part can be more problematic. Because we have a second-order denominator and depending on roots, we may have ripples on the passband. To clarify the behavior of the equalizer, consider the magnitude Bode plots given in Figure 2.7 with respect to the parameters $A\omega_e$ and ω_o. Here, the gain is given as $A = 10 \quad (20dB)$.

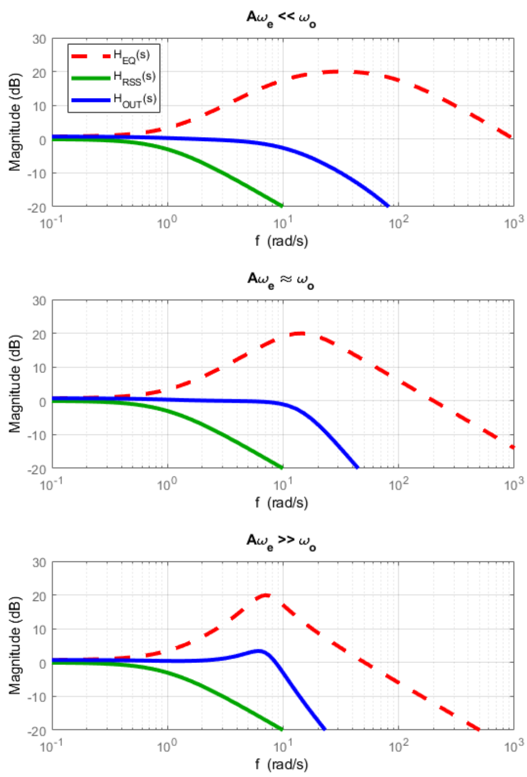

Figure 2.7. Three cases for the transfer function given by Equation(2.7).

Here, 3 distinct cases are observed:

(i) For $A\omega_e \ll \omega_o$, the available bandwidth of the Gm-Cell is not fully exploited, equalization factor which is defined as the ratio of equalized bandwidth to un-equalized bandwidth (received signal bandwidth) is about the gain: A.

(ii) For $A\omega_e \approx \omega_o$, the available bandwidth of the Gm-Cell is most efficiently used (without any ripple on the pass-band), the equalization factor is still about A.

(iii) For $A\omega_e \gg \omega_o$, in this case, the bandwidth is insufficient for ideal equalization. There is a ripple on the pass-band and the equalization factor is limited by also the bandwidth of Gm-Cell rather than simply by A. But for mild cases, the equalization factor could still be about A.

The general result of the above discussion is that the equalization factor is hugely defined by the gain given sufficient bandwidth. To further convince ourselves, consider the magnitude Bode plots given in Figure 2.8 for $A = 2, 10$ and 40 given a sufficient bandwidth of $\omega_o = 40 \times \omega_e$.

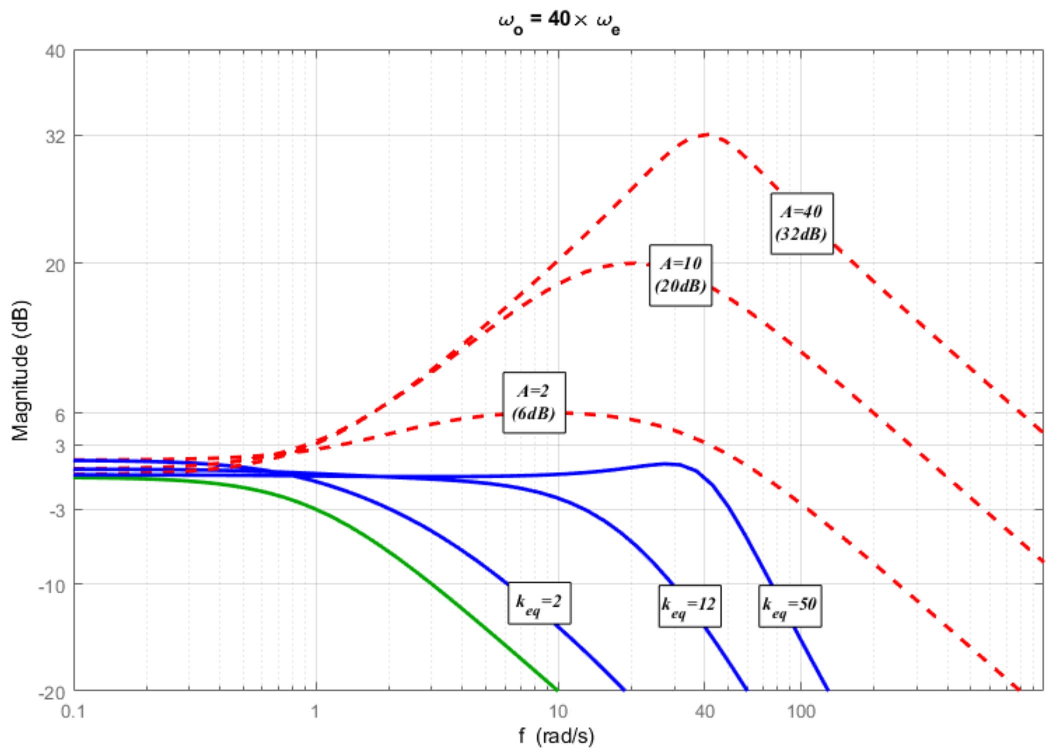

Figure 2.8. Equalization factor vs gain.

Here, observe that the equalization factors are $2, 12$ and 50 respectively. With respect to the gains, $2, 10$ and 40, we may conclude the relation $k_{eq} \approx A$. And also observe that as $A\omega_e \to \omega_o$, the equalization factor becomes a bit larger than A which is advantageous. But care should be taken not to have large ripples on the passband. In brief, one should prefer a response between (ii) or (iii) to most efficiently use a Gm-Cell. In the case of (iii), there is a chance of having ripples on the passband. But for a given maximum ripple criteria, the necessary parameters can be calculated. Now, let us summarize the assumptions:

- $A \gg 1$ (for a reasonable equalization),
- $\omega_o \gg \omega_e$

So, we can simplify the equalizer response given with Equation (2.7) as

$$\begin{aligned} H(s) &= \frac{1 + \cancel{1/A} + s\frac{1}{\omega_e}}{1 + \cancel{1/A^2} + s\left(\frac{1}{A\omega_e} + \cancel{\frac{1}{A^2\omega_o}}\right) + s^2\frac{1}{A\omega_e\omega_o}}, \\ &= \frac{1 + s\frac{1}{\omega_e}}{1 + s\frac{1}{A\omega_e} + s^2\frac{1}{A\omega_e\omega_o}}. \end{aligned}$$

For a given received signal spectrum $H_{RSS}(s) = \frac{1}{1+s\frac{1}{\omega_c}}$, the equalized spectrum becomes

$$\begin{aligned} H_{OUT}(s) &= H_{RSS}(s) \times H_{EQ}(s), \\ &= \frac{1}{1 + s\frac{1}{\omega_c}} \times \frac{1 + s\frac{1}{\omega_e}}{1 + s\frac{1}{A\omega_e} + s^2\frac{1}{A\omega_e\omega_o}}, (\omega_e = \omega_c), \\ &= \frac{1}{1 + s\frac{1}{A\omega_e} + s^2\frac{1}{A\omega_e\omega_o}}. \end{aligned}$$

This equation can be written as

$$H_{OUT}(s) = \frac{A\omega_e\omega_o}{s^2 + s\omega_o + A\omega_e\omega_o}. \tag{2.8}$$

Now consider that we have ripples on the passband. In that case, the poles of Equation(2.8) must be complex. The poles can be given as

$$\rho_{1,2} = \alpha \pm j\beta,$$
$$H(s) = \frac{\alpha^2 + \beta^2}{s^2 + 2\alpha s + \alpha^2 + \beta^2}.$$

Location where ripple occurs can be found by solving $\frac{\partial |H(j\omega)|}{\partial \omega} = 0$, which yields:

$$\omega_{ripple} = \sqrt{\beta^2 - \alpha^2}.$$

The amount of ripple becomes

$$|H(j\omega)|_{max} = \frac{\alpha^2 + \beta^2}{2\alpha\beta},$$

here, $\alpha^2 + \beta^2 = A\omega_e\omega_o$ and $2\alpha = \omega_o$,

$$|H(j\omega)|_{max} = \frac{A\omega_e\omega_o}{\omega_o\sqrt{A\omega_e\omega_o - \frac{\omega_o^2}{4}}} = \frac{A\omega_e}{\sqrt{A\omega_e\omega_o - \frac{\omega_o^2}{4}}}.$$

For a given 3dB maximum ripple criteria, one should solve $|H(j\omega)|_{max} \leq 3dB$, or equivalently, $|H(j\omega)|^2_{max} \leq 2$. Valid solution is given as

$$\omega_o \geq A\omega_e \times \left(2 - \sqrt{2}\right).$$

So, as a result, a bandwidth of $\omega_o \geq 0.6 \times A\omega_e$ would be sufficient for 3dB passband ripple criteria (or equivalently, $f_o \geq 0.6 \times Af_e$). Now let us calculate the equalization factor to clarify how it relates to the gain (A). Consider the equalized response $H_{OUT}(s)$, the equalized bandwidth can be found by solving $|H(j\omega)| = -3dB$, or equivalently, $|H(j\omega)|^2 = \frac{1}{2}$, which yields

$$\omega^2_{-3dB} = -\alpha^2 + \beta^2 + \sqrt{2(\alpha^4 + \beta^4)}.$$

In terms of parameters, we can write

$$\omega_{eq}^2 = A\omega_e\omega_o - \frac{\omega_o^2}{2} + \sqrt{\frac{\omega_o^4}{4} - A\omega_e\omega_o^3 + 2(A\omega_e\omega_o)^2}.$$

Consider the following cases:

(i) $A\omega_e \approx \omega_o$,

$$\omega_{eq} \approx A\omega_e \times \sqrt{\frac{1+\sqrt{5}}{2}}.$$

The equalization factor becomes

$$k_{eq} := \frac{\omega eq}{\omega_e} = A \times \sqrt{\frac{1+\sqrt{5}}{2}} \approx A, \qquad \left(\sqrt{\frac{1+\sqrt{5}}{2}} = 1.098\right).$$

(ii) $A\omega_e \gg \omega_o$,

$$\omega_{eq} \approx \sqrt{A\omega_e\omega_o \times (1+\sqrt{2})}.$$

This indicates that when ω_o is insufficient, equalized bandwidth is also limited by ω_o, not simply by A. Table 2.1 summarizes the conclusive result of these analyses.

Table 2.1. Results of hand analysis.

Parameter	**Requirement**	**Condition**	**Result**
ω_o	Minimum necessary bandwidth	$A \gg 1$ $R_p < 3dB$	$\omega_o \geq 0.6 \times A\omega_e$
k_{eq}	Relation to gain and bandwidth	$A \gg 1$ $\omega_o \approx A\omega_e$	$k_{eq} \approx A$

For our case, $f_e = [0.7 \quad 5]$MHz. Consider the equalization from $f_e = 5$MHz to $f_{eq} = 100$MHz, $k_{eq} = \frac{100}{5} = 20$. Thus, necessary gain for Gm-Cell $2A = 40V/V(32dB)$ and necessary bandwidth $f_o > 0.6 \times 20 \times 5$MHz $\Rightarrow f_o > 60$MHz.

2.2. Trade-Offs

Although we clarified the necessary gain and bandwidth of Gm-Cell, we have not yet determined the reasonable value for transconductance (it may affect both parameters). To clarify, consider the bandwidth-transconductance relation and edge frequency formula given as

$$\omega_o \propto g_m,$$
$$\omega_e = \frac{g_m}{C_{tune}}.$$

For a wider bandwidth, a larger g_m is preferred. But, this time the value of tuning capacitance increases, consequently the chip area. Different transconductance values (different Gm-Cells) may be preferred for gyrators and the main amplifier to adjust the ω_o and C_{tune} independently. But the number of parameters in the transfer function increases so much to handle. So for these reasons, we choose identical and a moderate value for g_m. For a given Gm-Cell topology, if the necessary gain is already obtained, g_m can be assessed by adjusting the bias current and observing the resulting bandwidth.

3. REALIZATION

Now we should realize a Gm-Cell with parameters: $2A = 40V/V(32dB)$ and $f_o > 60$MHz. And also Gm-Cell should have an STC (Single Time Constant) behavior as described in Figure 2.3(b). For that purpose, consider the feasible candidates for a Gm-Cell in Figure 3.1.

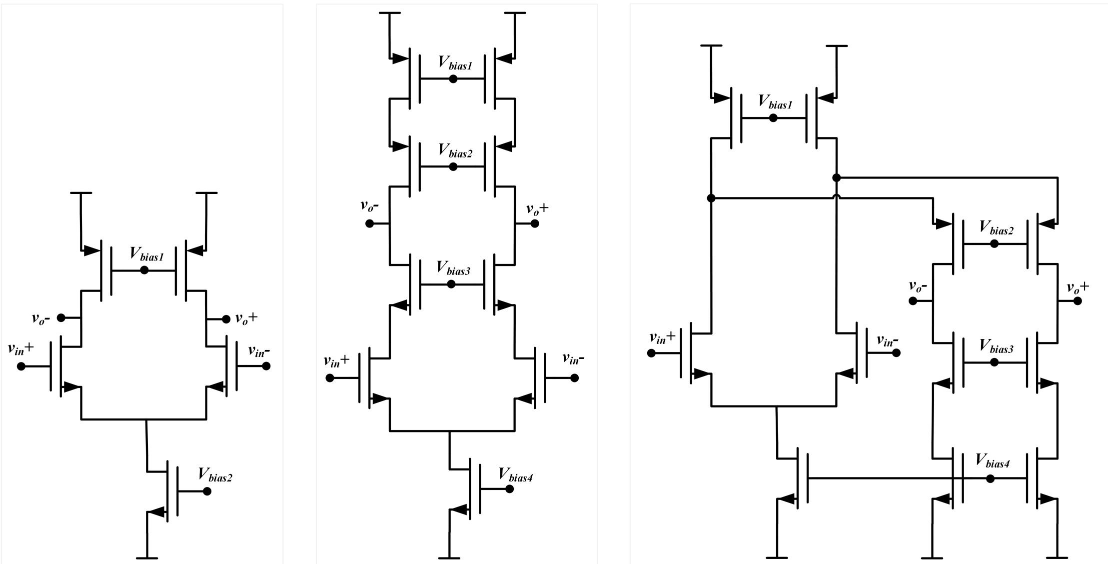

(a) (b) (c)

Figure 3.1. Basic Differential Amplifier (a), Telescopic Cascode Amplifier (b) and Folded Cascode Amplifier (c).

The most basic form of a Gm-Cell is shown in Figure 3.1(a), a MOSFET differential pair with active loads. Despite its easy implementation, the gain achievable with this circuit is not sufficient for our case. To boost the gain, a cascode structure given in Figure 3.1(b) can be used in exchange for bandwidth. But, with a low voltage power supply, VDS voltages of MOSFETs are limited as there are 5 MOSFETs stacked between the power supplies. To reduce the number of stacked transistors, we may use the folded cascode structure given in Figure 3.1(c). A detailed version of this circuit is given in Figure 3.2 with bias currents are shown.

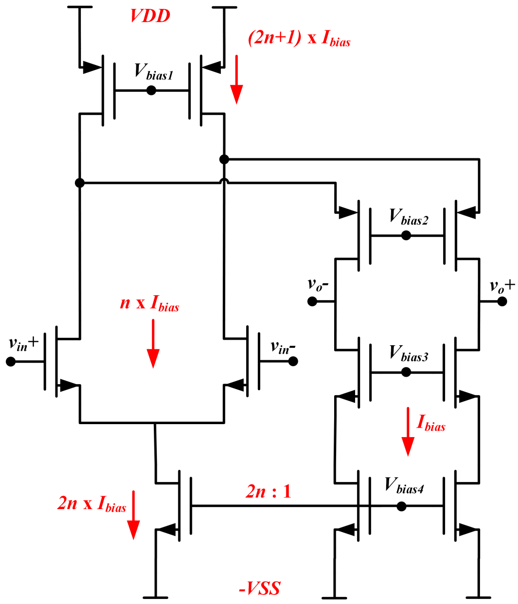

Figure 3.2. Bias currents for fully differential folded cascode amplifier.

In the actual usage of folded cascode structure, the number: n is chosen quite large to have high output resistance, thus high gain. But in our case, we need a moderate level of gain so we may choose $n = 1$. We realized the circuit using low-threshold (Low-VT) 130nm MOSFETs. As we are dealing with sub-micron MOSFETs, the general square model is not valid for hand analysis. As an alternative method, we employ simulation and graphical methods for the MOSFET with geometries given in Table 3.1 to obtain the necessary parameters using the relations given as

$$g_m = \frac{\partial I_{DS}}{\partial V_{GS}}, \quad r_o = \frac{\partial V_{DS}}{\partial I_{DS}}, \quad A = g_m r_o = \frac{\partial V_{DS}}{\partial V_{GS}}.$$

Table 3.1. MOSFET sizes for simulation and graphical analysis.

MOSFET SIZES: W/L [μm]			
Amplifiers		Current Sources (CS)	
NMOS Differential	PMOS Common Gate	Top PMOS CS	Bottom NMOS CS
6.0 / 0.16	1.0 / 0.12	5.0 / 0.4	1.0 / 0.4

With the aid of simulation and graphical analysis results, the schematic is drawn as shown in Figure 3.3 with the CMFB (Common-Mode-Feed-Back) circuit included (right-hand-side of the schematic).

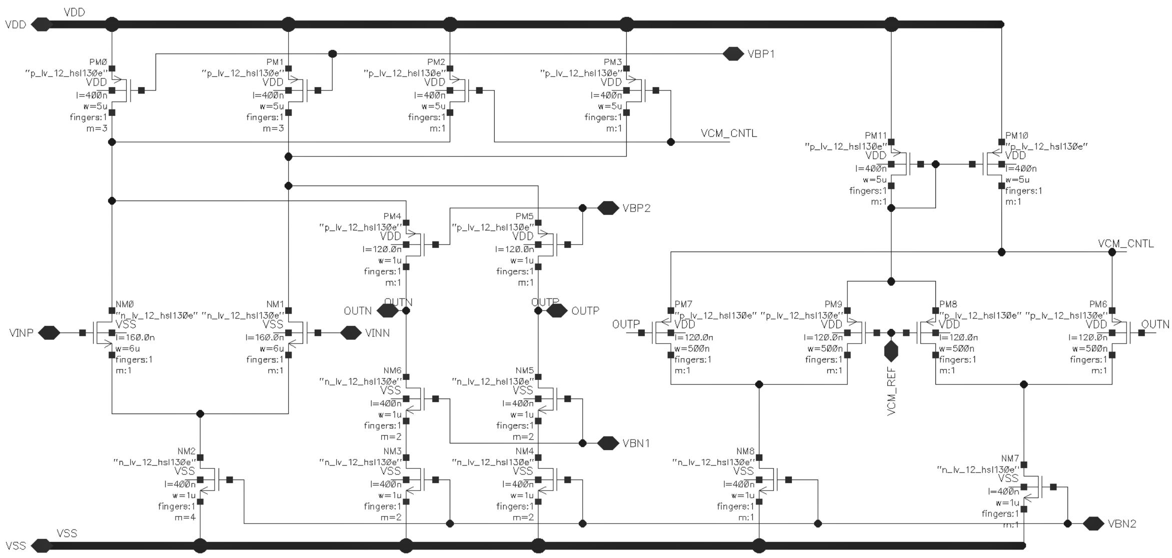

Figure 3.3. Schematic of fully differential folded cascode amplifier with CMFB.

Common-mode feedback is carried out by controlling 1/4 of the bias current. Observe that the top PMOS current source is implemented by $m = 4$ transistors, 3 of them are biased by a fixed gate voltage while the gate of the last transistor is controlled by the CMFB circuit. Here, we should remark another good reason for choosing folded cascode structure over telescopic cascode. Consider the gyrator circuit in Figure 2.4, where the output of one Gm-Cell is connected to the input of another. The level of common-mode voltage at these nodes is important and must be well defined for the proper operation of the Gm-Cells. Ideally, the common-mode voltage at the output of Gm-Cell is between the supply voltages. In case split supplies are used, $V_{CM,out} = 0V$. Which can be satisfied easily in folded cascode structure.[1] The symbol for the Gm-Cell and biasing circuit is given in Figure 3.4. Figure 3.5 shows the test bench for the Gm-Cell.

[1] A similar issue which is well described by Behzad Razavi as "The drawback of telescopic cascode is the difficulty in shorting its inputs and outputs" in his book: "Design of Analog CMOS Integrated Circuits Second Edition"

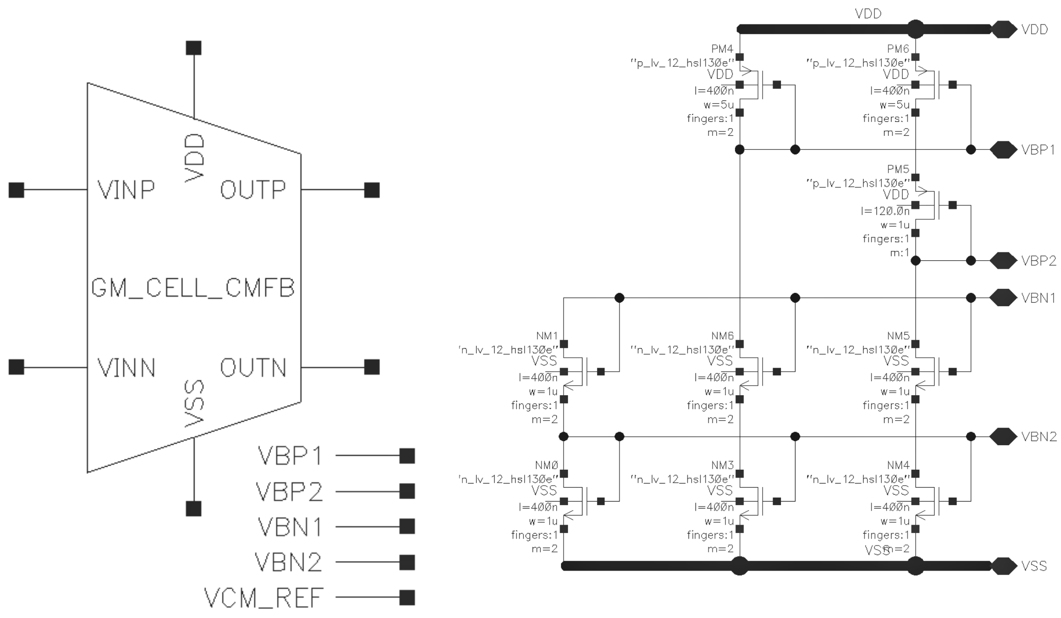

(a) (b)

Figure 3.4. Symbol (a) and bias circuit (b) for the Gm-Cell.

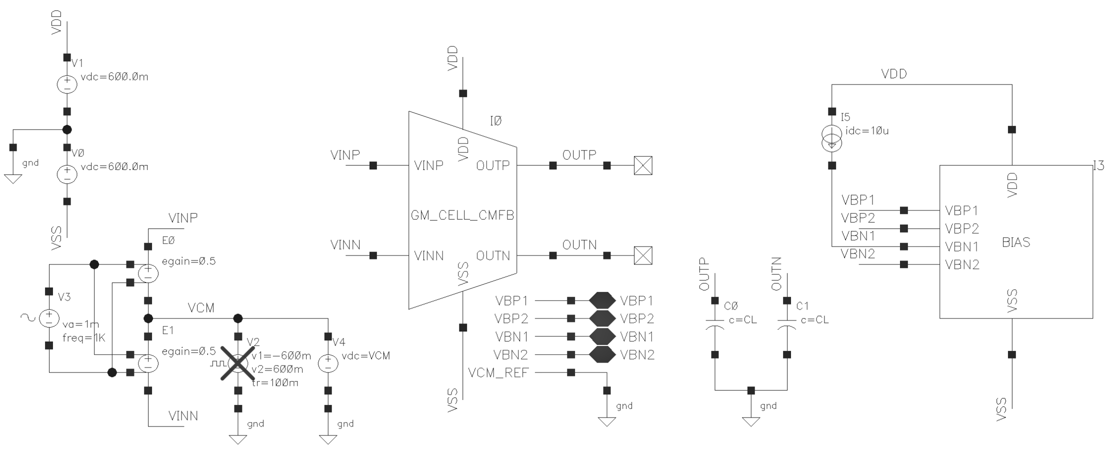

Figure 3.5. Test bench for the Gm-Cell.

In the following figures, we show the frequency response, input/output common-mode voltage ranges, and parameter extractions. The circuit is simulated with a bias current of $I_{bias} = 10\mu A$ and with a split supply voltage of $\pm 0.6V$. We can crudely approximate the transconductance of the circuit by $g_m = \frac{2i}{V_{ov}}$, $\quad V_{ov} \approx 0.2V$, $g_m \approx \frac{2\times 10\mu A}{0.2V} = 100\mu S$. Figure 3.6(a) shows the variation of the gain as a function of input common-mode voltage. For a $\pm 5\%$ gain variation, we may say, the proper input common-mode range is $[-300 \quad 400]mV$. In that case, the corresponding output common-mode voltage range is $[-50 \quad 50]mV$ as shown in Figure 3.6(b). Figure 3.6(c) shows the frequency responses of the Gm-Cell for input common-mode voltages of $V_{CM,in} = -300 : 100 : 400 \quad mV$, results are also summarized in Table 3.2. We show the frequency response for $V_{CM,in} = 0V$ in Figure 3.6(d) again to show that the nominal gain and bandwidth of the Gm-Cell is $34dB(50V/V)$ and 77MHz. Additionally, Gm-Cell has (approximate) STC network behavior up to 1GHz.

$$Slope_{(100M \to 1G)} = 8.9 - 30.1 = -21.2dB/decade.$$

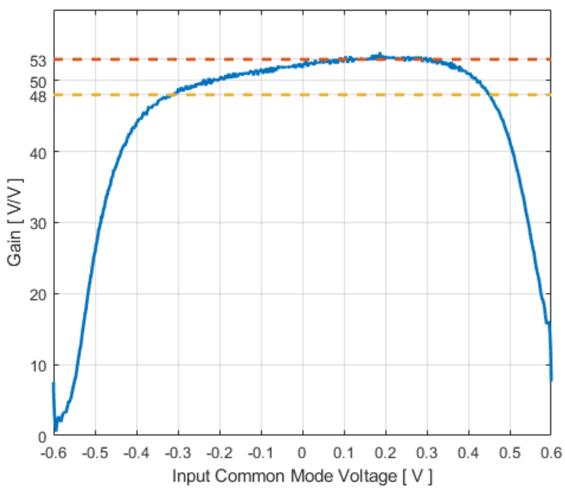

(a) Gain vs $V_{CM,in}$.

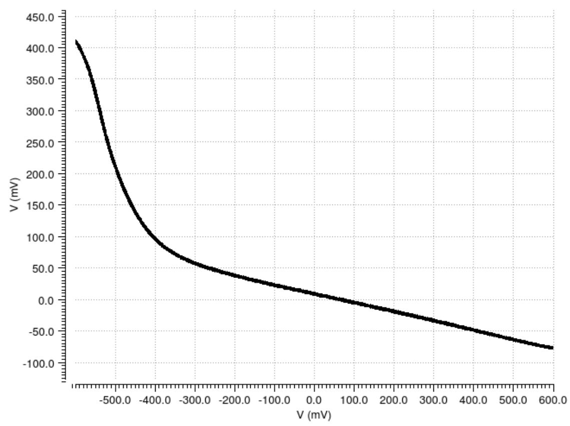

(b) $V_{CM,in}$ vs $V_{CM,out}$.

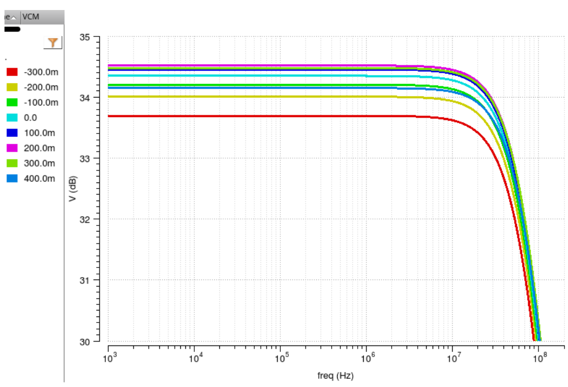

(c) Frequency responses for various $V_{CM,in}$ values.

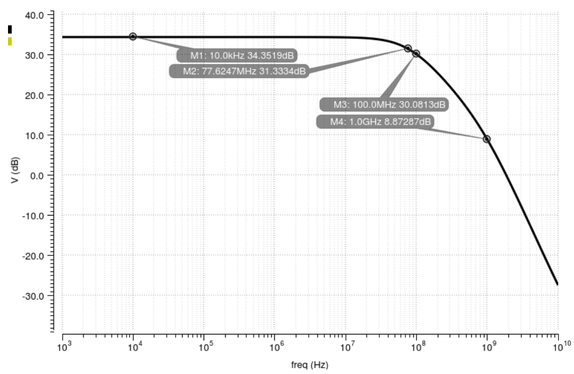

(d) Frequency response for $V_{CM,in} = 0V$.

Figure 3.6. Simulation results.

Table 3.2. Gain and bandwidth of Gm-Cell as a function of $V_{CM,in}$.

$V_{CM,in}$ [mV]	Gain:2A [dB]	Bandwidth: f_o [MHz]
-300	33.70	58.88
-200	34.01	75.86
-100	34.21	77.10
0	34.35	77.27
100	34.46	77.62
200	34.51	78.34
300	34.47	79.43
400	34.15	83.18

3.1. Parameter Extraction

We designed the folded cascode amplifier without definitely knowing parameters, g_m, r_o and c_o. But we can experimentally extract these parameters. The below list summarizes the methods to extract them.

- Observe the short circuit transconductance by putting a low impedance load at the output (a large capacitor). This method is used to ensure that the majority of the signal current is bypassed by the output load impedance which is lower than the equivalent output impedance of the amplifier.
- By using the extracted g_m and $2A = 2g_m r_o \Rightarrow r_o = \frac{2A}{2g_m}$.
- By using the extracted r_o and bandwidth from frequency response, $A(s) = \frac{2g_m r_o}{1+sr_o c_o} \Rightarrow f_{-3dB} = \frac{1}{2\pi r_o c_o} \Rightarrow c_o = \frac{1}{2\pi r_o f_{-3dB}}$.

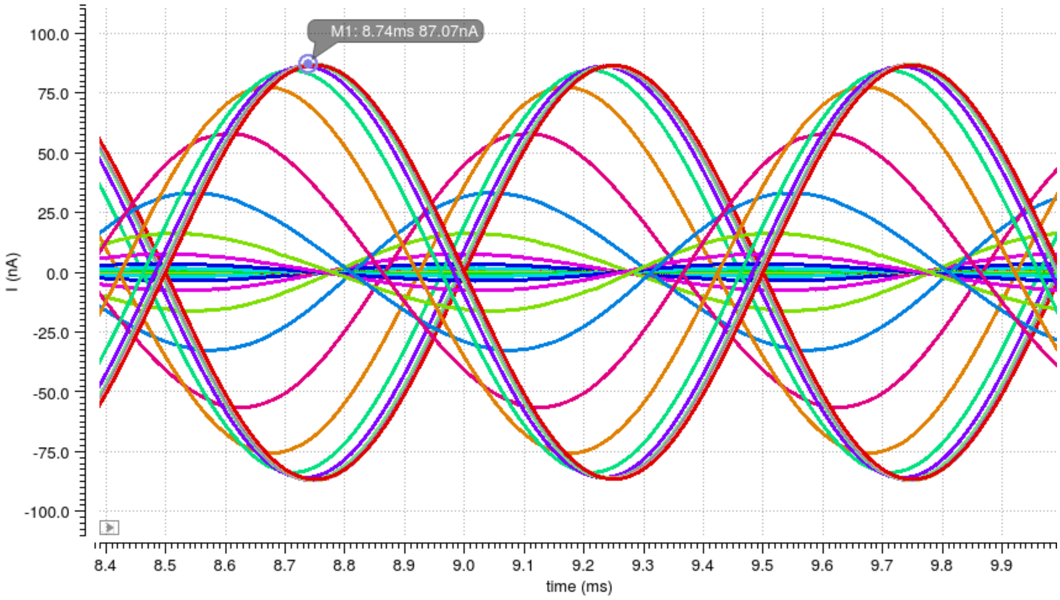

Figure 3.7. Output load signal currents for various loads.

Figure 3.7 shows the output load signal currents for $1mV@1kHz$ input sinusoidal signal and for various output loads $C_{LOAD} = 1pF \rightarrow 1\mu F$. As can be seen, maximum signal current is $i_{sc} = 87nA$, which corresponds to a short-circuit-transconductance of

$$g_m = \frac{87nA}{1mV} = 87\mu S,$$
$$r_o = \frac{2A}{2g_m} = \frac{52.2V/V}{2 \times 87\mu S} = 300k\Omega,$$
$$c_o = \frac{1}{2\pi r_o f_{-3dB}} = \frac{1}{2\pi \times 300k\Omega \times 77.27M} = 6.87fF.$$

3.2. Validation of the Parameters

To validate the parameters extracted, let us first put an output capacitance that is equal to the equivalent output capacitance of the amplifier. In this case, we expect the bandwidth to drop by 1/2. Figure 3.8(a) shows that the bandwidth drops to 38.9MHz with $C_{LOAD} = c_o = 6.87fF$ $\left(\frac{77.6M}{2} = 38.8M\right)$.

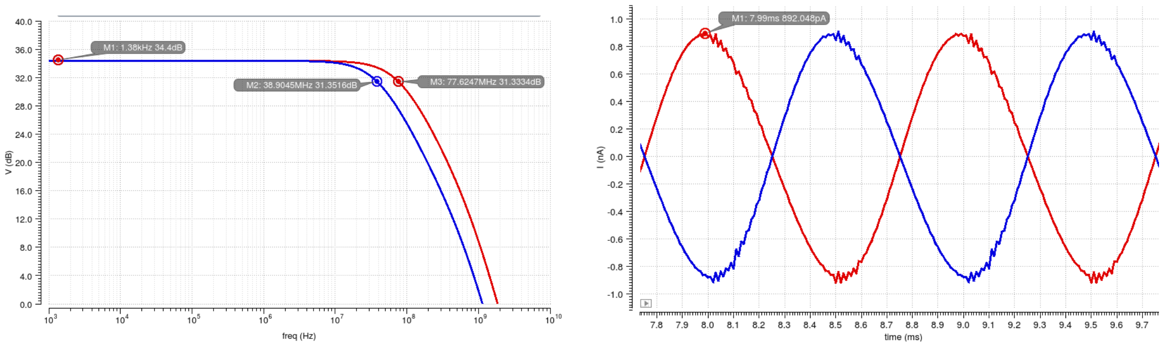

(a) Frequency response with $C_{LOAD} = c_o$ (blue). (b) Load currents for $Z_{LOAD} = 99 \times z_o$.

Figure 3.8. Simulation results for validation.

Secondly, let us put an output load that has 99 times larger impedance than the equivalent output impedance of the amplifier. This time we expect a load current which is 1/100 of the short circuit signal current. Consider the following

$$
\begin{aligned}
r_o &= 300k\Omega, \\
X_{co} &= \frac{1}{2\pi f c_o}(@1kHz) = 23.2G\Omega, \\
z_o &= r_o \parallel X_{co} \approx r_o = 300k\Omega, \\
Z_{LOAD} &= 99 \times z_o, \\
C_{LOAD}(@1kHz) &= \frac{1}{2\pi f Z_{LOAD}} = 5.36pF.
\end{aligned}
$$

Figure 3.8(b) shows the load currents for $C_{LOAD} = 5.36pF$ and $1mV@1kHz$ input sinusoidal signal. Here, $i_{LOAD} \approx 0.89nA \quad \left(\frac{i_{sc}}{100} = \frac{87nA}{100} = 0.87nA\right)$.

3.3. Layout and Post Layout Simulation for Gm-Cell

Following precautions taken into account to minimize the non-ideal effects of layout design:

- As the amplifier is fully differential, signal pairs are drawn as symmetric as possible to reduce the mismatches and hereby input-referred offsets. Adequate symmetry also suppresses the effect of common-mode noise and even-order nonlinearities.

- A semi-guard ring is employed around PMOS and NMOS regions for reasons, such as, to reduce substrate noise coupling and prevent latch-ups (a full guard ring is hardly possible due to the folded cascode structure).

Figure 3.9 shows the layout of Gm-Cell. The frequency response of the Gm-Cell is shown in Figure 3.10 for schematic and post-layout. The gain is almost the same around 34dB (50V/V) for both cases and bandwidth dropped after layout as expected.

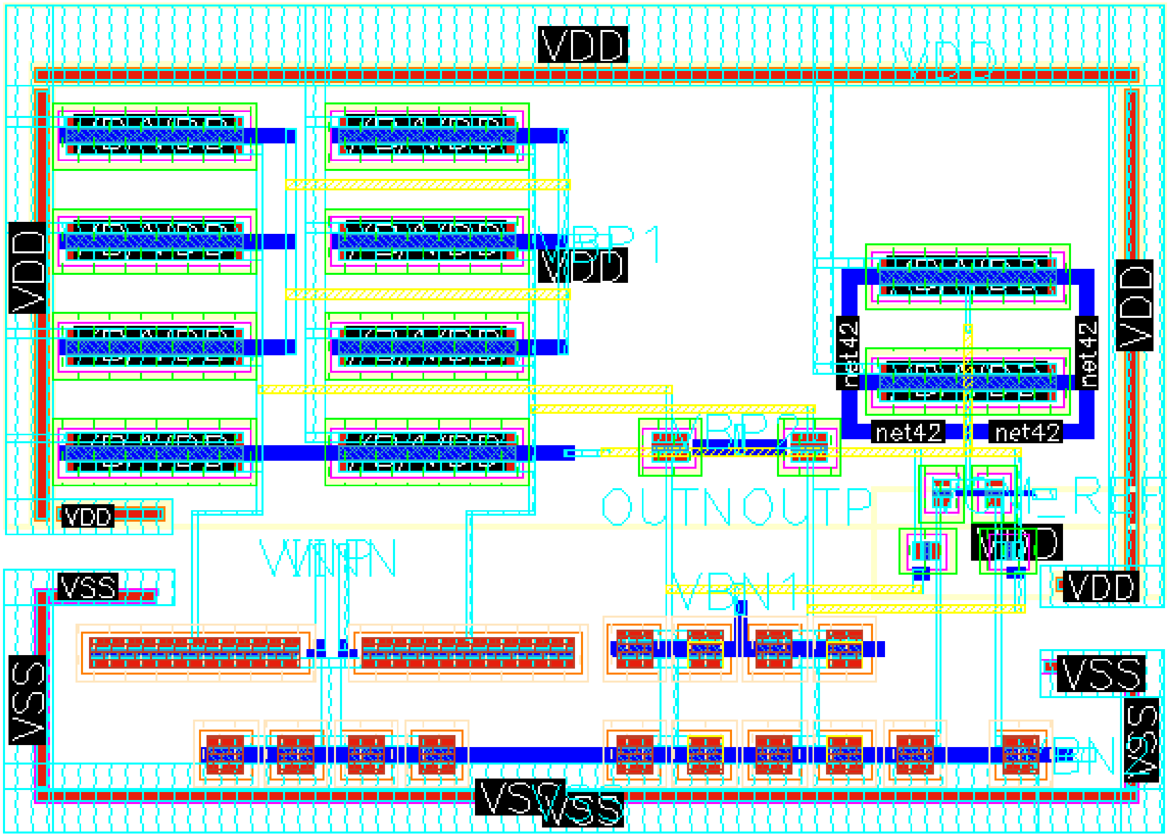

Figure 3.9. Layout of Gm-Cell.

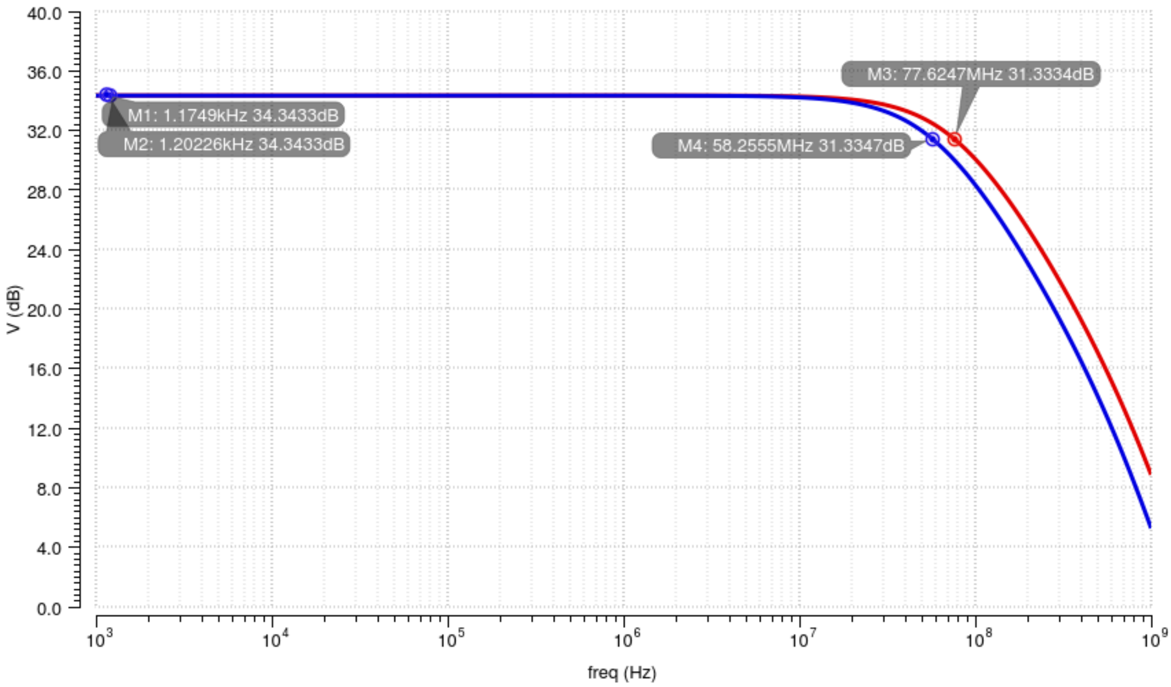

Figure 3.10. Frequency response of Gm-Cell for schematic (red) and post-layout (blue).

3.4. Realization of Equalizer

Now we can simulate the equalizer topology. First, let us calculate the necessary tuning capacitance values. The tuning frequency range is $f_e = [0.7 \quad 5]$MHz and corresponding capacitances can be calculated as

$$f_e = \frac{g_m}{2\pi C_{tune}} \Rightarrow C_{tune} = \frac{g_m}{2\pi f_e},$$
$$C_{tune,max} = \frac{87\mu S}{2\pi \times 0.7M} = 19.78pF,$$
$$C_{tune,min} = \frac{87\mu S}{2\pi \times 5M} = 2.77pF.$$

We employ a 3-Bit capacitor to add adjustability to the equalizer's edge frequency. To calculate the necessary 1-Bit capacitor value, consider that the minimum value tuning capacitor is directly connected to the tuning node as default (C_{DF}). Other 3-bit capacitor corresponds to 8 distinct tuning capacitance from 0 to $7 \times C_{bit}$ by C_{bit}

steps. So the minimum and maximum tuning capacitances become

$$C_{tune,min} = C_{DF} = 2.77pF,$$
$$C_{tune,max} = C_{DF} + 7 \times C_{bit} = 19.78pF,$$

and 1-Bit unit capacitance can be calculated as

$$C_{bit} = \frac{C_{tune,max} - C_{tune,min}}{2^3 - 1} = \frac{19.78 - 2.77}{7} = 2.43pF.$$

Calculated tuning capacitance values and corresponding edge frequencies are summarized in Table 3.3.

Table 3.3. 3-Bit Capacitors and corresponding edge frequencies.

Bits				C_{tune}	f_e
D0	D1	D2	DF	[pF]	[MHz]
0	0	0	1	2.77	5.00
1	0	0	1	5.20	2.66
0	1	0	1	7.63	1.81
1	1	0	1	10.06	1.37
0	0	1	1	12.50	1.11
1	0	1	1	14.92	0.93
0	1	1	1	17.35	0.80
1	1	1	1	19.78	0.70

Figure 3.11 and Figure 3.12 show the equalizer schematic and the frequency response of the equalizer, the results are also given in Table 3.4.

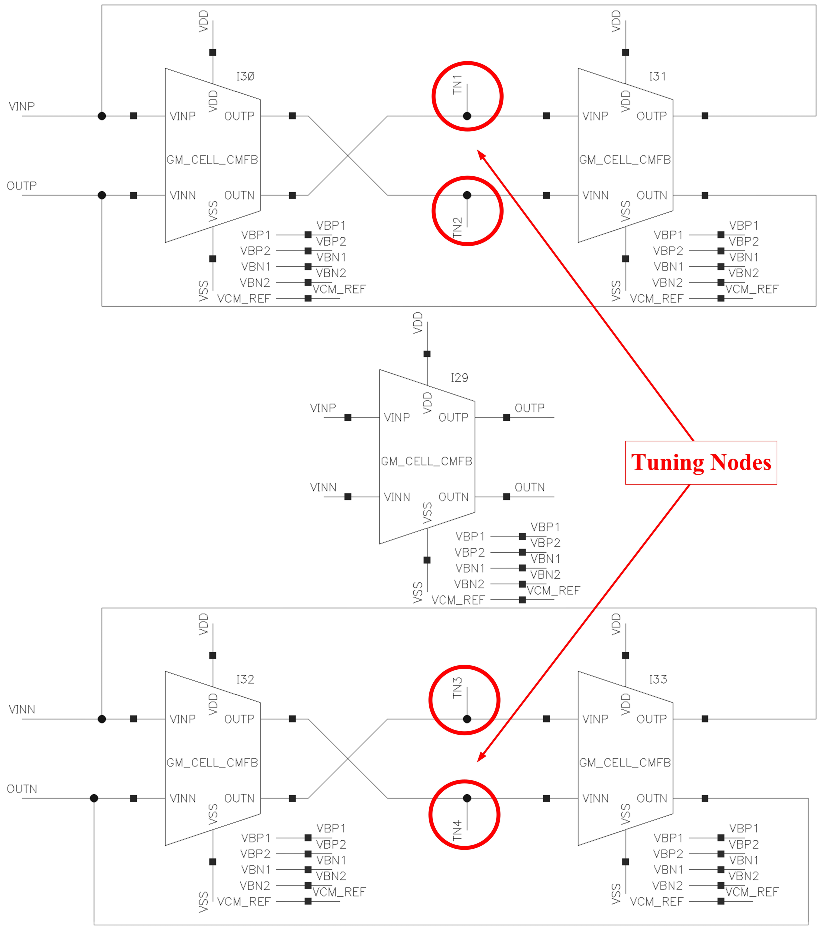

Figure 3.11. Schematic of the PEQ.

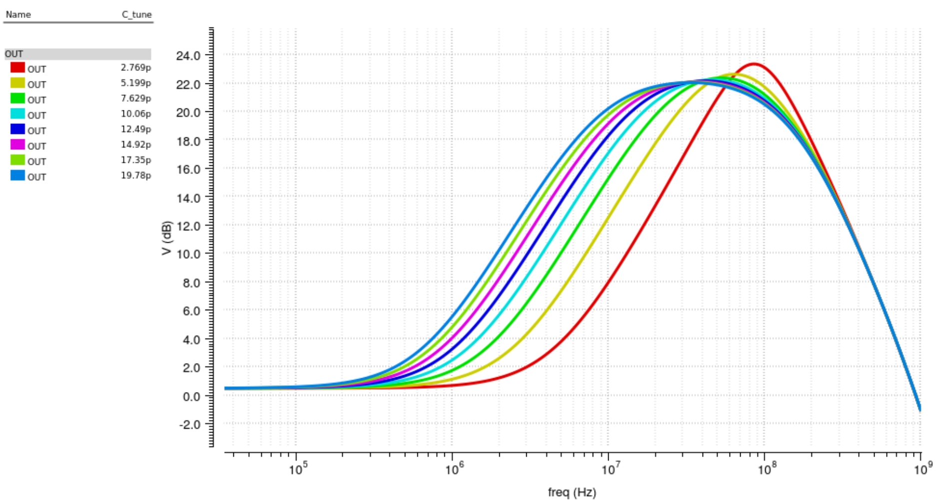

Figure 3.12. Frequency response of the PEQ for various C_{tune} values.

Table 3.4. Summary of simulations results.

C_{tune} [pF]	f_e [MHz]		Effective g_m [μS]	f_e^* [MHz]
	Calculated	Simulated		After Re-calculation
2.77	5.00	4.63	80.6	5.03
5.20	2.66	2.51	81.8	2.72
7.63	1.81	1.71	82.1	1.86
10.06	1.37	1.31	82.7	1.42
12.50	1.11	1.05	82.7	1.15
14.92	0.93	0.88	82.7	0.96
17.35	0.80	0.76	83.1	0.83
19.78	0.70	0.67	83.0	0.73

It seems from the simulation results that the effective g_m is different from the short-circuit-transconductance. To match for the calculated edge frequencies, we may choose the effective transconductance as $g_{m,eff} = 80\mu S$ and recalculate the tuning capacitances as

$$
\begin{aligned}
C_{tune,max} &= \frac{80\mu S}{2\pi \times 0.7M} = 18.19pF, \\
C_{tune,min} &= \frac{80\mu S}{2\pi \times 5M} = 2.54pF, \\
C_{bit} &= \frac{18.19 - 2.23}{7} = 2.23pF.
\end{aligned}
$$

Re-simulated results are given on the right-hand side of Table 3.4.

3.4.1. The layout of Equalizer and Post Layout Simulations

Figure 3.13 and Figure 3.14 show the layout and post-layout simulation of the equalizer. After the layout, edge frequencies are almost the same but at high frequencies, there are deviations from the schematic simulation as expected.

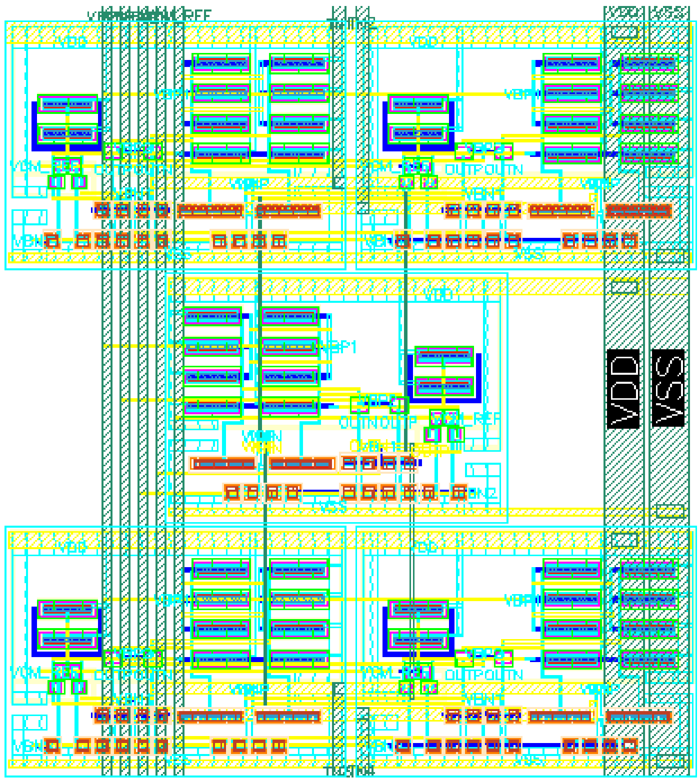

Figure 3.13. Layout of the PEQ.

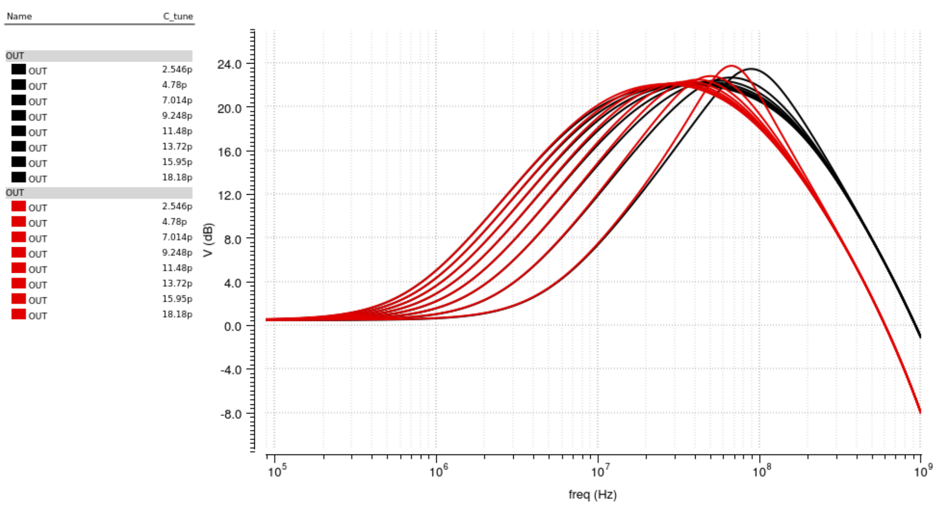

Figure 3.14. Frequency response of the PEQ for schematic (black) and post-layout (red).

3.4.2. Layout with Tuning Capacitors

Tuning capacitors are realized using unit Capacitor-Switch blocks as shown in Figure 3.15. Using unit capacitor-switch blocks provides more precise tuning capability and speeds up the layout design. Switches are realized using basic transmission gates. For a given state of operation of the equalizer, each switch is either on or off. Dynamic operation of the switches is not much of a concern. So, they are designed in the simplest form (for example, no dummy switches are used).

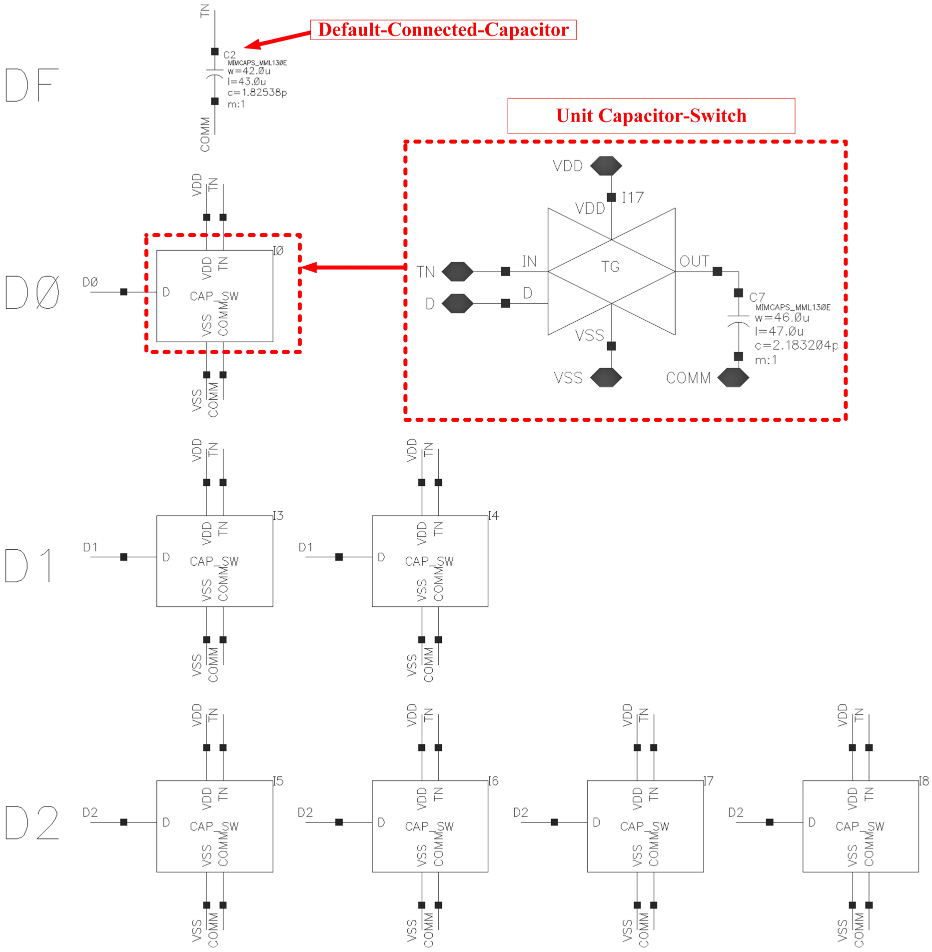

Figure 3.15. Schematic of tuning Capacitor-Switch Block.

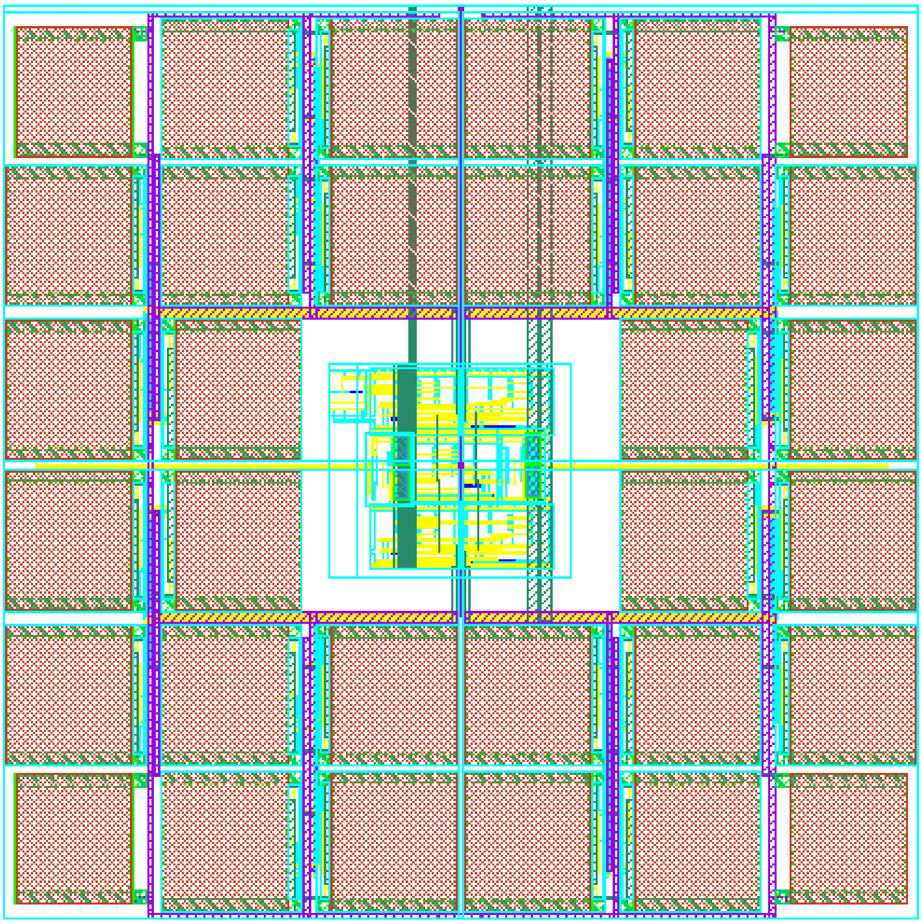

Figure 3.16. The complete layout of the PEQ with tuning capacitors.

An extra capacitance appears at tuning nodes due to layout which is around 0.7pF-1pF depending on the state of bits. So, post-layout corrections are performed as follows

$$C^*_{tune,max} = 18.19 - 1 = 17.19pF,$$
$$C^*_{tune,min} = 2.54 - 0.7 = 1.85pF,$$
$$C^*_{bit} = \frac{17.19 - 1.85}{7} = 2.19pF.$$

Figure 3.16 shows the complete layout of the equalizer. The total chip area is $\sim 340 \times 340\mu m^2$. The majority of the chip area is occupied by the tuning capacitances. MIM (Metal-Insulator-Metal) capacitors are used as they exhibit better capacitance density (farad per meter square) compared to the other types of capacitors (MOM, MOS, etc.). Post-layout simulation results are given in Figure 3.17 and Table 3.5.

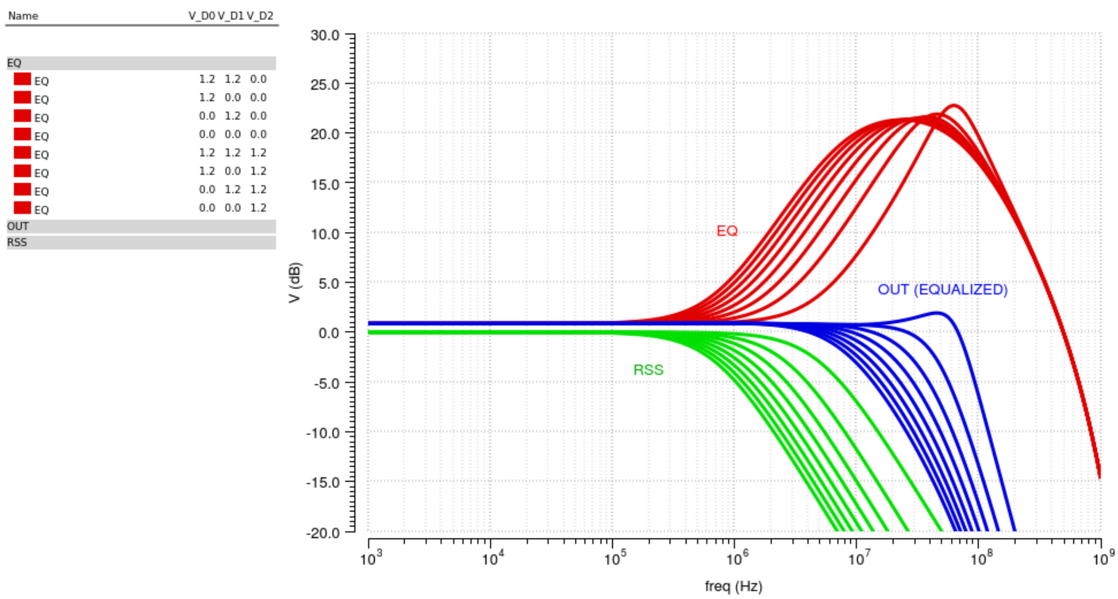

Figure 3.17. Input signal spectrum (green), the frequency response of PEQ (red), and equalized signal spectrum (blue).

Table 3.5. Summary of simulation results for the complete layout of PEQ.

C_{tune} [pF]	f_c [MHz]	f_e [MHz]	f_{eq} [MHz]	R_p [dB]	Equalization Factor $k_{eq} = \frac{f_{eq}}{f_c}$
2.54	5.01	5.13	79.4	1.1	15.8
4.78	2.69	2.67	42.6	-	15.8
7.01	1.82	1.81	26.3	-	14.4
9.25	1.38	1.36	18.6	-	13.4
11.48	1.12	1.09	14.1	-	12.5
13.72	0.93	0.92	11.5	-	12.3
15.95	0.81	0.78	9.6	-	11.8
18.19	0.71	0.69	8.3	-	11.7

Here:

- f_c : Cut-off frequency of received signal spectrum (un-equalized bandwidth),
- f_e : Edge frequency of the PEQ which is mathced for corresponding f_c,
- f_{eq} : Equalized signal spectrum (equalized bandwidth),
- R_p : Pass-band ripple for equalized bandwidth,
- k_{eq} : Equalization factor: ratio of equalized bandwidth to un-equalized bandwidth.

3.5. Performance Evaluation

To assess the actual performance of the equalizer, it is best to use eye diagrams. For that purpose, consider the test bench in Figure 3.18 and the following simulated test procedure:

- The limited bandwidth behavior of the signal at the receiver side is modeled by a simple differential RC-LPF with a cut-off frequency of 5MHz.
- Equalizer's edge frequency is adjusted to corresponding cut-off frequency by setting tuning bits as: $D_0D_1D_2D_F = 0001$ which yields an edge frequency of 5.13MHz and equalizes the signal spectrum to 80MHz (Figure 3.19).
- Basic On-Off Keying (OOK) modulated signal with $\pm 100mVpp$ is applied from the signal source with worst-case bit scenario is included (0-1, 1-0 sequence at each clock cycle).
- A periodic clock jitter with 10% RMS of clock period is also included in the simulation to obtain more realistic eye diagrams.
- Simulation is performed for 100MBits, 200MBits and 250MBits as shown in the following figures.

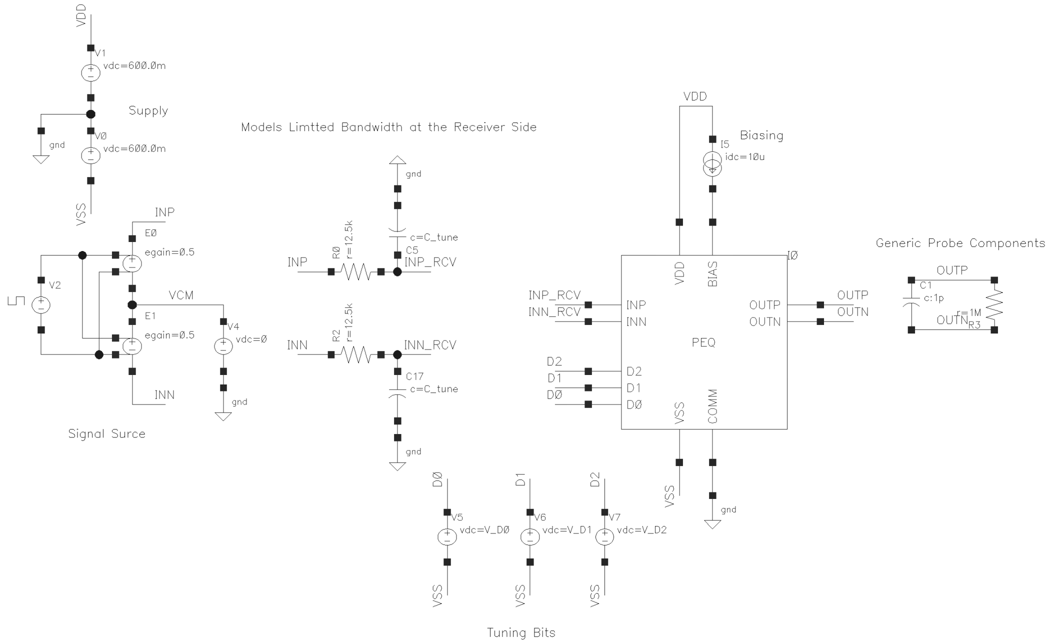

Figure 3.18. PEQ simulated Test-Bench (Post-Layout).

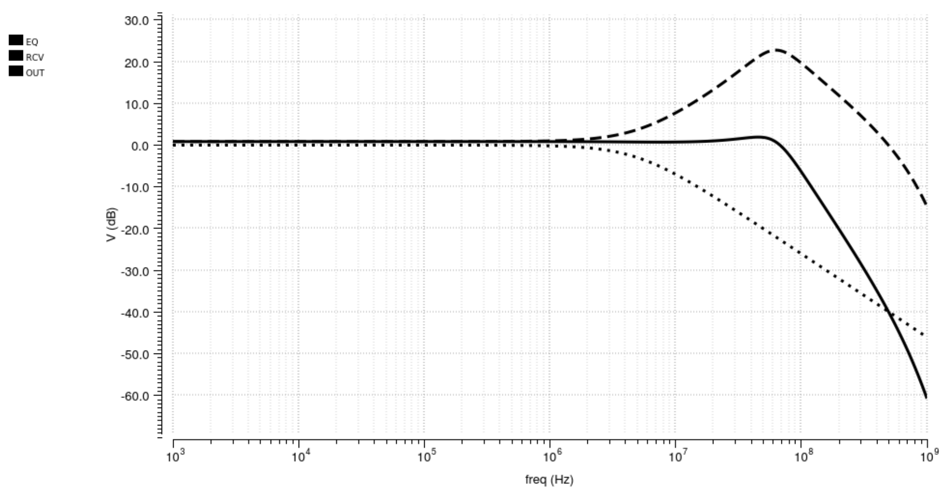

Figure 3.19. Frequency responses for equalization from 5MHz to 80MHz.

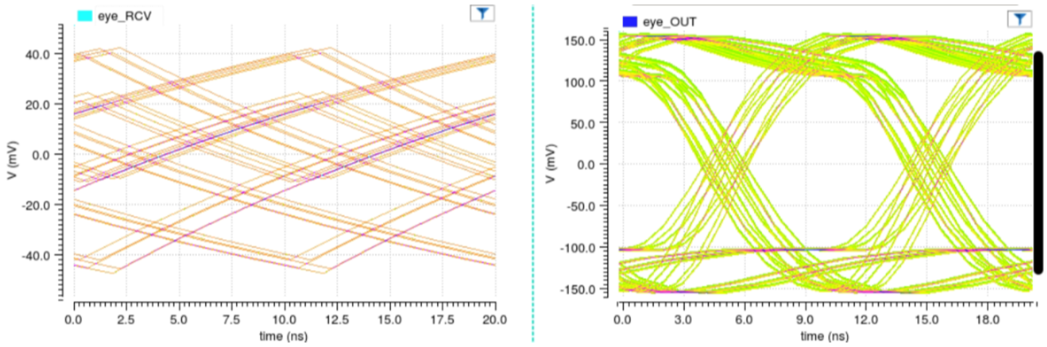

(a) Data Rate=100MBits.

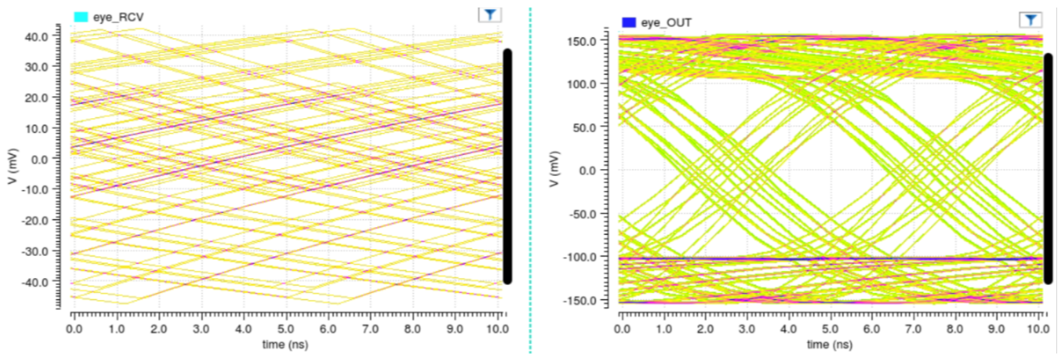

(b) Data Rate=200MBits.

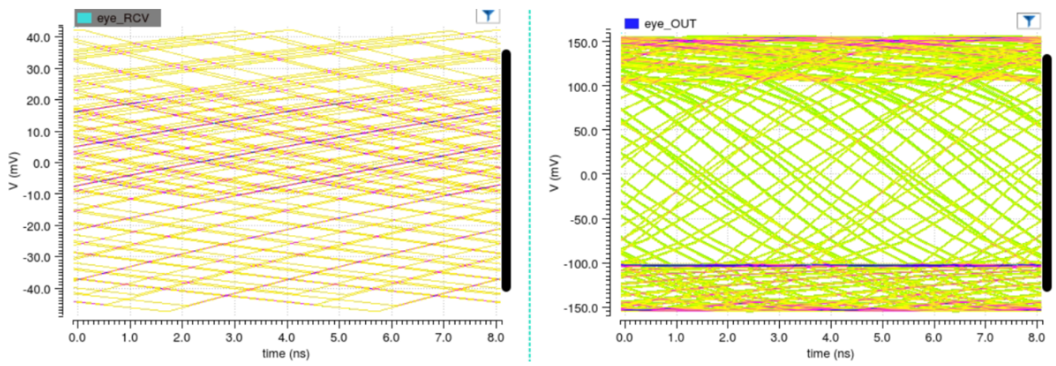

(c) Data Rate=250MBits.

Figure 3.20. EYE diagrams for various data rates, un-equalized (left) and equalized (right).

Figures show that it is possible to have open eye diagrams for data rates up to 200MBits. Beyond this data rate, it is not possible to obtain a clear eye diagram.

4. CONCLUSION

In this work, a Gm-C-based post equalizer is proposed and realized using 130nm low-VT MOSFETs. Post layout simulations show that the equalizer provides at least tenfold post equalization and it's possible to achieve data rates up to 200MBits given that a 5MHz modulation bandwidth is available at the receiver side.

The chip layout of the proposed equalizer is $340 \times 340\mu m^2$ with the majority of the area is occupied by tuning capacitors. This is one disadvantage of using Gm-C topology while precise tuning of the edge frequency is possible. This is true for on-chip applications where capacitors can be more precisely implemented than other passive components such as resistors and inductors.

Input and output buffers are also included in the layout design to make equalizer response more robust. Because the proposed equalizer works given two conditions. First, the signal source must have low output impedance, and secondly, at the output, there should not be an additive load (especially capacitive, such as generic probe components). Buffers satisfy both conditions.

The total power dissipation of the circuit is $10mW(8mA@1.2V)$ while we should note that the majority of power is consumed by input/output buffers. The equalizer itself consumes only $240\mu W(200\mu A@1.2V)$

Lastly, in this proposed topology, we employed identical Gm-Cells for both the main amplifier and gyrators. This provides a simple characteristic equation that is suitable for hand analysis. One may choose different Gm-Cells for the main amplifier and gyrators. In this case, the designer is free to choose smaller g_m for gyrators, thus smaller tuning capacitors (and smaller layout) and larger g_m for the main amplifier to have wider bandwidth. But, in this case, the characteristic equation becomes too complex for hand analysis and consequently, the designer loses insight into how the equalizer behaves with respect to these parameters. For the reasons we described above, we preferred using identical Gm-Cells, showed with post-layout simulations that proposed topology can be realized with reasonable chip area and provide at least tenfold post equalization.

REFERENCES

1. Wang, Y., L. Tao, X. Huang, J. Shi and N. Chi, "8-Gb/s RGBY LED-Based WDM VLC System Employing High-Order CAP Modulation and Hybrid Post Equalizer", *IEEE Photonics Journal*, Vol. 7, No. 6, pp. 1–7, 2015.

2. Wang, Y., L. Tao, Y. Wang and N. Chi, "High Speed WDM VLC System Based on Multi-Band CAP64 with Weighted Pre-Equalization and Modified CMMA Based Post-Equalization", *IEEE Communications Letters*, Vol. 18, No. 10, pp. 1719–1722, 2014.

3. Le Minh, H., D. O'Brien, G. Faulkner, L. Zeng, K. Lee, D. Jung, Y. Oh and E. T. Won, "100-Mb/s NRZ Visible Light Communications Using a Postequalized White LED", *IEEE Photonics Technology Letters*, Vol. 21, No. 15, pp. 1063–1065, 2009.

4. Li, H., X. Chen, B. Huang, D. Tang and H. Chen, "High Bandwidth Visible Light Communications Based on a Post-Equalization Circuit", *IEEE Photonics Technology Letters*, Vol. 26, No. 2, pp. 119–122, 2014.

5. Li, X., B. Hussain, L. Wang, J. Jiang and C. P. Yue, "Design of a 2.2-mW 24-Mb/s CMOS VLC Receiver SoC With Ambient Light Rejection and Post-Equalization for Li-Fi Applications", *Journal of Lightwave Technology*, Vol. 36, No. 12, pp. 2366–2375, 2018.

6. Fujimoto, N. and S. Yamamoto, "The Fastest Visible Light Transmissions of 662 Mb/s by a Blue LED, 600 Mb/s by a Red LED, and 520 Mb/s by a Green LED Based on Simple OOK-NRZ Modulation of a Commercially Available RGB-Type White LED Using Pre-Emphasis and Post-Equalizing Techniques", *The European Conference on Optical Communication (ECOC)*, pp. 1–3, 2014.

7. Kısacık, R., T. Erkınacı, M. Y. Yağan, A. E. Pusane, M. Uysal, T. Baykaş,

G. Dündar and A. D. Yalçınkaya, “Opto-Electronic Receiver System with Post-Equalization for Visible Light Communications”, *28th Signal Processing and Communications Applications Conference (SIU)*, pp. 1–4, 2020.

8. Le Minh, H., D. O’Brien, G. Faulkner, L. Zeng, K. Lee, D. Jung and Y. Oh, “High-Speed Visible Light Communications Using Multiple-Resonant Equalization”, *IEEE Photonics Technology Letters*, Vol. 20, No. 14, pp. 1243–1245, 2008.

9. Zhang, H., A. Yang, L. Feng and P. Guo, “Gb/s Real-Time Visible Light Communication System Based on White LEDs Using T-Bridge Cascaded Pre-Equalization Circuit”, *IEEE Photonics Journal*, Vol. 10, No. 2, pp. 1–7, 2018.

10. Li, G., F. Hu, Y. Zhao and N. Chi, “Enhanced Performance of a Phosphorescent White LED CAP 64QAM VLC System Utilizing Deep Neural Network (DNN) Post Equalization”, *IEEE/CIC International Conference on Communications in China (ICCC)*, pp. 173–176, 2019.

11. Wang, L., X. Wang, J. Kang and C. P. Yue, “A 75-Mb/s RGB PAM-4 Visible Light Communication Transceiver System with Pre- and Post-Equalization”, *Journal of Lightwave Technology*, Vol. 39, No. 5, pp. 1381–1390, 2021.

12. Huang, H., C. Wang, C. Huang, H. Wu and H. Wang, “Visible Light Communication System with 815 MHz-Modulation Bandwidth Based on Micro-Size Light-Emitting Diode and Post-Equalization Circuit”, *15th China International Forum on Solid State Lighting: International Forum on Wide Bandgap Semiconductors China (SSLChina: IFWS)*, pp. 1–4, 2018.

13. Grubor, J., S. C. J. Lee, K.-D. Langer, T. Koonen and J. W. Walewski, “Wireless High-Speed Data Transmission with Phosphorescent White-Light LEDs”, *33rd European Conference and Exhibition of Optical Communication - Post-Deadline Papers*, pp. 1–2, 2007.

14. Ha, Y., W. Niu and N. Chi, "Post Equalization Scheme Based on Deep Neural Network for a Probabilistic Shaping 128 QAM DFT-S OFDM Signal in Underwater Visible Light Communication System", *18th International Conference on Optical Communications and Networks (ICOCN)*, pp. 1–3, 2019.

15. Li, Z., F. Hu, G. Li, P. Zou, C. Wang and N. Chi, "Convolution-Enhanced LSTM Neural Network Post-Equalizer Used in Probabilistic Shaped Underwater VLC System", *IEEE International Conference on Signal Processing, Communications and Computing (ICSPCC)*, pp. 1–5, 2020.

16. Yuan, F., J. Wang, W. Yu and J. Ren, "A Post-Equalizer Based on Dual Self-Attention Network in UVLC System", *IEEE Photonics Journal*, Vol. 13, No. 2, pp. 1–11, 2021.

17. Aliparast, P., A. Khoei and K. Hadidi, "A Novel Fully-Differential Gm-C Filter Structure for Communication Channel Equalizer", *14th International Conference on Mixed Design of Integrated Circuits and Systems*, pp. 209–214, 2007.

18. Tang, Z., "A 100 MHz Gm-C Analog Equalizer for 100Base-TX Application", *6th International Conference on Solid-State and Integrated Circuit Technology. Proceedings*, Vol. 1, pp. 240–242, 2001.

19. Galembeck, R., J. de Lima and M. Schneider, "A Gm-C Bump Equalizer for Low-Voltage Low-Power Applications", *IEEE International Symposium on Circuits and Systems*, Vol. 1, pp. I–797, 2004.

20. Huang, J. and R. R. Spencer, "A CMOS Gm-C Analog Pre-Equalizer for 1000BASE-T Analog Receive Filters", *IEEE Asian Solid-State Circuits Conference*, pp. 173–176, 2005.